NUREG/CR-5099
SAND88-0052

Evaluation of Materials of Construction for the Reinforced Concrete Reactor Containment Model

Prepared by G. A. Knorovsky, P. W. Hatch, M. R. Gutierrez

Sandia National Laboratories

Prepared for
U.S. Nuclear Regulatory
Commission

NUREG/CR-5099
SAND88-0052
R1, RD

Evaluation of Materials of Construction for the Reinforced Concrete Reactor Containment Model

Manuscript Completed: August 1988
Date Published: September 1988

Prepared by
G. A. Knorovsky, P. W. Hatch, M. R. Gutierrez

Sandia National Laboratories
Albuquerque, NM 87185

Prepared for
Division of Engineering
Office of Nuclear Regulatory Research
U.S. Nuclear Regulatory Commission
Washington, DC 20555
NRC FIN A1249

Abstract

This report summarizes the chemical analysis, metallography, and tensile test results obtained from steel materials and welds used in the construction of a 1/6-scale model reinforced concrete nuclear reactor containment. The purpose of building such a model is to experimentally verify the ability of numerical models to predict deformation and failure in full-size containments. Naturally, the predictions of such models are strongly influenced by the constitutive models used for the containment materials. The program reported here was intended to provide such data. Besides providing tensile test data on the sheet, plate, and rebar materials used for dome, cylinder, cylinder inserts, reinforcements, and penetrations, pull tests on several weld geometries have been obtained. Standard tensile test data derived from load vs. extensometer output records (engineering stress vs engineering strain) are supplemented with true stress vs true strain data collected by measuring actual cross sectional areas during interrupted tensile tests. Additionally, "r" value measurements (ratio of width to thickness strain) which can be used to provide information about anisotropic multiaxial flow conditions are derived from the true strain data and reported. A small number of tests that included holds at constant load levels were also performed and analyzed to yield ambient temperature creep equations. Finally, conditions resulting from construction practices (such as residual stresses and the Bauschinger effect) that may affect the prediction of yield and fracture stresses from this data are briefly discussed.

Table of Contents

List of Figures

List of Figures (cont'd)

List of Figures (cont'd)

List of Figures (cont'd)

List of Tables

Introduction

As part of Sandia National Laboratories' Reactor Containment Integrity Program, an approximately 1/6th scale model of a generic reinforced concrete reactor containment building was designed, built, comprehensively instrumented, and tested to failure by internal pressurization. Materials and construction practices were intended to duplicate those used in full-size containments as much as possible. The purpose behind this effort is to study the behavior of such structures under beyond-design-basis conditions, and furthermore to verify the capability of existing computer codes to predict such behavior. Because the predictions of such computer codes are dependent upon accurate material mechanical response models, it was necessary to measure mechanical properties for the materials of construction. This report is intended to document the extensive data gathering effort which was conducted in response to this need, and as such will be a supplement to the overall documentation package reporting on the program. Examples of *every* material or weld in the containment were not tested; however a broad range representative of most of the steel construction was evaluated. Concrete material properties are covered in a separate report [1]. Included in the body of this report are standard engineering stress/strain data and representative curves, supplemental true stress/strain data obtained to strains beyond the maximum load, derived values of the ratio between true width and thickness strains (the "r" value), ambient temperature creep data, chemical analyses, descriptions of how the data were obtained, and finally discussion on how the uniaxial data measured can be applied to the multiaxial stress and strain condition of the actual containment.

Chemical Analyses

Emission spectroscopy results obtained from the sheet and plate materials and reinforcing bars ("rebar") are summarized in Table I (note that the materials are defined by their thicknesses or diameters in the tables which follow; their locations in the containment model are defined below). Specifications under which the materials were purchased include: (1) liner (0.07" cylinder or bottom, and 0.09" dome materials): ASME SA-414 Grade D, (2) 0.2" liner insert: ASME SA-516 Grade 60, (3) large penetration sleeves (1.3" reduced to 0.5"): ASME SA-516 Grade 60, and (4) rebar: ASTM A-615. Supplemental requirements instituted by the constructor on the SA-414 liner material required that it be fully killed and made to fine grain practice. Analysis of the chemistries shown in Table I indicates that the A-414 materials were somewhat unusual in that they were killed with Al only, instead of the more usual Si or Si plus Al practice. Of all

the materials tested, only the dome material did not exhibit a sharp yield point. Interestingly, the cylinder material, with nearly identical composition, did exhibit a sharp yield point. With respect to meeting specification requirements, all the materials except for the 0.2" SA-516 are within specification. The SA-516 exceeds the allowed maximum limitation on Mn of 0.90 wt.%. Possibly this material was procured in larger thickness and reduced to its 0.2" value; the Mn specification limit increases to 1.20 wt.% for material exceeding 0.5". The rebar all appears to be A-615 grade 60 material. The 6mm bar was manufactured to an European standard, though it appears to meet all A-615 grade 60 chemical and tensile requirements.

Tensile Test Results

Standard sheet tensile specimens of 0.5" gauge width by 2" gauge length by material thickness (or 0.25", whichever was less) were machined from sheet and plate materials provided. Only the material taken from 1.3" thick plate had all four sides of the gauge length machined; the others taken from sheet were machined on the edges only, with the as-rolled surfaces left as received (oxidized from atmospheric exposure). In addition to pre-dished dome material (0.09"), post-dished (cold worked) dome material was also tested. Tensile specimens were taken in both longitudinal and transverse directions with respect to the rolling direction. At least two specimens were pulled for each combination of material and orientation tested. All specimens were tested at ambient temperature. The nominal strain rate was 10^{-3} sec.$^{-1}$. Engineering stress/strain data for the tensile specimens are summarized in Table II, and representative curves for each material are given in Figures 1-4. It should be noted that the small values of the standard deviation given in Table II for several of the materials may not be representative of the variation that would actually be expected with a greater number of specimens. It would be prudent to choose a pooled value, which for the yield and ultimate stresses are: 0.52 and 0.42 ksi respectively.

True stress/strain data are summarized in Figures 5-8 and Table II. The true stress/strain data were determined by stopping the tensile test at intervals and measuring the actual cross sectional area at five locations along the gauge length using dial calipers. These measurements are taken to beyond the point at which diffuse necking begins (past the maximum load condition), and so provide true strain data to higher strains than are usually obtainable by conversion from engineering stress/strain curves. Until local necking occurs near failure (such data would deviate from the straight line through data at lower strains on the ln true stress/ln true strain plot), this enables good measurement of stresses and strains. A Bridgman-type correction [2] was not applied to compensate for the effect of non-axial stress components. It

was noted that the actual strains measured (given by $\varepsilon = \ln[A_o/A]$, where A = instantaneous area and A_o = original specimen cross sectional area) were significantly different from the average strains measured by the extensometer even at the smallest true strains (~5%) measured.

Sheet metal butt welds were tested in the cross-weld orientation (for which load data, and not stress, is reported), and in the longitudinal (all-weld-metal) orientation. The cross-weld specimens were not machined on all four sides, thus the weld reinforcement prevented a uniform cross section, and failure always took place outside the weld region. The all weld metal specimens were fully machined to a gauge cross section of ~0.25" wide by ~0.05-~0.08" thick depending on the weld size. In addition to the sheet metal butt seam welds, samples of various other weld geometries were made. These specimens were nominally 1" wide, and were pulled to failure. If the failure was not in the weld fusion or heat affected zone, this region was machined down to a reduced width, and another sample pulled, at which time failure did occur in the weld region. Details of these geometries, and the manner in which they were loaded are given in Figure 9. Maximum loads for both the full and reduced width samples are given in Table III, as is the tensile data for the all weld metal specimens and the stud weld specimens. Representative load-strain or load-elongation cross-weld and engineering stress-strain all weld metal curves are shown in Figures 10 - 18.

As in the case of the cross-weld samples, load vs. extension data only are provided for the rebar materials, which were not machined to a uniform section, but were tested as received. Load data are given in Table IV, and representative load vs engineering strain curves are given in Figures 19-22.

"r" value data is summarized in Table II (refer to the discussion section for a definition of "r"). Linear curves were fit to data plots of true width and thickness strain vs true longitudinal strain as shown in Figures 23-26 (note that the "R" value given on these figures refers to the goodness of fit of the straight line through the data points). The first of the two "r" values given in Table II refers to a value obtained at the maximum load as suggested in ASTM E-517 (obtained by inserting the longitudinal true strain at maximum load in the linear best-fit equations for true width and thickness strain, and taking the ratio of these values), and the second by taking the ratio of the slopes of the best-fit curves. Because the straight lines did not in general go exactly through the origin, the two values differ. Where the values differ, the authors prefer the ratio of the slopes value, as the straight lines should go through the origin. Small systematic measurement errors are reflected more in the intercept than in the slope; furthermore, the most accurate

data occurs at larger strains but before local necking takes place, simply because of the precision of the calipers used for area measurement.

Metallographic Results

Welds were sectioned metallographically to determine if any porosity or other defects were present. With the exception of the stud welds to the 0.2" material, no serious problems were noted. These latter stud welds exhibited poor consistency, with extensive porosity and cracking in some of the welds, while others broke the shaft of the stud during tensile testing (at ~1600 lbs.). These conditions are shown in Figures 27 & 28. The load-extension data (see Table III) also exhibited large scatter, and several of the welds were broken off in handling. Stud welds to the thinner sheet showed consistently good strength, with only minor porosity being present. Examples of the other sheet metal welds are shown in Figures 29-36.

Discussion

Elastic Properties-Previous data gathering for reactor containment model testing [3] also included determining values of the elastic moduli and Poisson's ratio. Since values obtained in the earlier work showed little variation from handbook values, such tests were not conducted.

Multiaxial Yield and Failure Criteria-The standard tensile test data summarized in this report provide information on the behavior of materials under uniaxial stress conditions. However, as the testing of the model containment is under multi-axial conditions, yield and failure criteria for multiaxial conditions must be chosen in order to compare computer code predictions with experiment. A common choice for the yield condition is the Von Mises criterion. This assumes isotropic behavior of the material; however, it may be extended to anisotropic materials if certain material constants are known (via Hill's analysis, as explained in [4]. The complexity of the mathematical equations which describe the yield locus and hence, required number of material constants, increases depending upon upon how anisotropic the material is. For the special case of planar isotropy (an important case for sheet material, which corresponds to equal uniaxial yield stresses in the rolling and transverse directions, but not in the thickness direction) only one constant needs to be determined. This constant, the plastic strain ratio or "r" value, is the ratio of strain in the transverse direction to the tensile axis, i.e. the width strain, to the thickness strain, with the ratio averaged over specimens taken parallel to the rolling direction, transverse direction and 45 degrees to rolling direction. It relates the ratio of the yield stress in the thickness direction: σ_3 to

that in plane: σ_1 (the yield stress in the rolling direction) or σ_2 (the yield stress in the transverse direction) by the equation:

$$\sigma_3/\sigma_1 = \sigma_3/\sigma_2 = [(1 + r)/2]^{1/2}$$

The usefulness of this relation becomes evident when it is realized that the yield stress under balanced biaxial tensile loading is equivalent to the compressive yield stress in the thickness direction (the two stress states differ only by a hydrostatic compressive stress equal to the yield stress in the thickness direction, and since the yield locus is assumed insensitive to hydrostatic pressure, the values are equivalent). An approximate "r" value can be obtained from the interrupted true stress/strain test data obtained in this program (no tests were conducted in the 45 degree direction as is required in the ASTM E-517 Standard). Values of this parameter for the various materials of construction are tabulated in Table II. Within the accuracy of the measurements no significant difference in "r" between the rolling and transverse directions was noted. In agreement with this the values of yield stress for the rolling and transverse directions in Table II can also be seen to be insignificantly different. Hence the planar isotropy condition appears to hold reasonably well. The values of r obtained are significantly different from 1.0 in nearly all cases; however, they are not so different that an analysis based upon isotropic behavior would be seriously affected.

In addition to these considerations for predicting biaxial yielding, two other influences need to be considered. The first is that any welded vessel will contain substantial residual stresses of both tensile and compressive nature. Secondly, since the deformation of the sheet and plate materials necessary to shape them into their final cylindrical or spherical forms was accomplished without subsequent annealing, the Bauschinger effect must be taken into account. Both of these influences will be expected to wane as a few percent deformation occurs, and they will not influence fracture (assuming that ductile fracture occurs).

Beyond the yield condition, empirically-determined Formability Limit Curves are more useful for predicting failure under biaxial loading conditions. Data for sheet steels of similar grades to that tested has been measured by Hecker [5]. An example of his data is shown in Fig 37. As may be seen in Fig. 37, the minimum condition of strain is usually near to the plane strain condition ($\varepsilon_2 = 0$; ε_1 & $\varepsilon_3 \neq 0$). Formability limits found in this manner assume that proportional straining is occurring; changing the strain path from other than radially outward from the origin can invalidate the limits given. Fortunately, for non-proportional straining where the

loading increases monotonically the limits tend to be conservative. Other investigators [6] have found that the ratio of the true plane strain ductility to the true uniaxial strain ductility is ~0.7 for a large range of steels of varying strengths. The maximum uniaxial true strains measured by the interrupted straining technique are summarized in Table II.

Determining a triaxial failure criterion analogous to the biaxial Forming Limit Curves is a non-trivial task. It is known that ductility is greatly reduced as the ratio of hydrostatic tensile to deviatoric stresses is increased [7]. Since failure of the test vessel will probably be found due to fracture initiation at a flaw or structural discontinuity anyway, it is questionable if a triaxial failure criterion for homogeneous material is really useful. Thus, it would probably be more appropriate to apply fracture mechanics considerations. No fracture mechanical testing was included in this program, though material has been archived should it become desirable in the future.

Variation of Weld Properies-The data for sheet weld metal as presented in Table III is divided into categories of size and weld position. Category choices were made by performing an analysis of variance on the data for yield stress (or load, for cross-weld specimens) and ultimate tensile stress (or maximum load) versus thickness and position of weld. Those found significantly different were separated and reported individually; otherwise data was grouped. At least four weld processes (Shielded Metal Arc, Gas Metal Arc, Gas Tungsten Arc and Capacitor Discharge Stud Welding) were specified in the construction of the vessel.

Model Containment Test Procedure vs Tensile Testing Procedure-The standard tensile test procedure is performed under monotonic loading conditions, whereas the model test involves a series of load increases followed by varying length hold periods. Since it is known that carbon and nitrogen can diffuse at room temperatures, it was felt desirable to check for evidence of strain ageing in the construction materials, and the effect it might have on the stress-strain relations. Two types of tests provided this data. First, the interrupted straining tests which gathered true strain data provided qualitative information on whether a load jump occurred upon reloading. However, since these were not optimum for gathering quantitative data, and none were performed on the rebar, a few computer-controlled tensile tests in which 4, 5 or 10 ksi (in engineering stress) load increments followed by constant load ageing steps (for 30 minutes) were also performed. The interrupted straining tests showed that only the Si/Al killed materials seemed to show evidence of ageing during the hold intervals. However, the load controlled tests did not seem to exhibit any such behavior. Instead, these

tests showed that after the creep strain interval the flow stress increased abruptly to the level which would be expected at the strain accumulated regardless of whether it was accumulated during monotonic loading or as a consequence of the interrupted loading path. This behavior is demonstrated in Figures 38-42 (the slight discontinuities seen in the monotonic loading specimens are an artifact of changing extensometer strain sensitivity during the test). The engineering strains accumulated during the constant load hold periods are plotted as log/log plots in Figures 43-47 as a function of engineering stress level and time. The strain data seem to be well-represented by a simple equation of the form:

$$\log \varepsilon = A + B \log t$$

The coefficients A and B are plotted as a function of stress level for each of the five major material types in Figure 48. Readers are cautioned that extrapolation of these equations beyond the stress, strain and time limits given by the data endpoints in Figures 43-47 may be questionable, as they are only obtained from curve-fitting and are not model-based. It was noteworthy that the amount of creep strain increased rapidly as the ultimate load was approached, and several specimens actually failed during their creep load holds. A value of the failure strain was not obtained as it exceeded the strain shut off limit of the software controlling the test (14%).

Summary

This report summarizes the chemistries and mechanical properties of materials of construction (including welds) for the 1/6-scale model reinforced-concrete reactor containment model tested in July of 1987 by Sandia National Laboratories' Containment Integrity Division. Measured properties reported included: 1) engineering yield and ultimate stresses and strains determined from monotonic tensile tests, 2) true stress/strain values to beyond maximum load determined from interrupted load tensile tests, and 3) creep strain accumulated during special programmed loading tests. Further, a measure of the yield surface anisotropy, the "r" value, or plastic strain ratio was also determined approximately. Additional comments concerning the materials of construction, the quality of welds, and the effect of other phenomena on the yield behavior were also noted. Should further testing be necessary, quantities of the materials will be archived for a reasonable length of time.

Bibliography

1. Horschel, D.S., Design, Construction, and Instrumentation of a 1/6-Scale Reinforced-Concrete Containment Building, NUREG/CR-5083, SAND88-0030, Sandia National Laboratories, Albuquerque, NM 87185, to be published.

2. Polakowski, N.H., Ripling, E.J., Strength and Structure of Engineering Materials, Prentice-Hall, Englewood Cliffs, NJ, 1966, p 278.

3. Reese, R.T., Horschel, D.S., Design and Fabrication of a 1/8-Scale Steel Containment Model, NUREG/CR-3647, SAND84-0048, Sandia National Laboratories, Albuquerque, NM 87185, February 1985, Appendix C.

4. Backofen, W.A., Deformation Processing, Addison-Wesley Publishing Co., Reading, MA, 1972, Chapters 2 & 3.

5. Hecker, S.S., "Experimental Studies of Sheet Stretchability", in Formability: Analysis, Modeling, and Experimentation, ed. by Hecker, S.S., Ghosh, A.K., and Gegel, H.L., AIME, New York, NY, 1978, pp 150-182.

6. Clausing, D.P., "Effect of Plastic Strain State on Ductility and Toughtness", Intl. J. of Fracture Mech., (6), 1970, p 71.

7. Le Roy, G., Embury, J.D., Edward, G., Ashby, M.F., "A Model of Ductile Fracture Based on the Nucleation and Growth of Voids", Acta Met., (29), 1981, pp 1509-1522.

Table I - Chemical Compositions

	<-----sheet/plate------>					<---------rebar--------->		
thickness or nom. dia.:	0.07"	0.09"	0.2"	1.3"	6mm	No.3 3/8"	No. 4 4/8"	No.5 5/8"
C	0.17	0.15	0.21	0.16	0.21	0.44	0.46	0.43
Mn	0.73	0.70	1.04	1.21	1.14	0.71	0.93	1.01
Si	<0.01	<0.01	0.18	0.23	0.46	0.15	0.19	0.15
S	0.009	0.006	0.021	0.015	0.018	0.041	0.03	0.039
P	0.015	0.018	0.011	0.011	0.027	0.022	0.01	0.024
Ni	<0.01	<0.01	<0.01	0.20	0.03	0.11	0.07	0.08
Cr	0.02	0.02	0.02	0.20	0.02	0.16	0.10	0.10
Mo	<0.01	<0.01	<0.01	0.05	<0.01	0.03	0.01	0.02
Cu	<0.01	0.02	<0.01	0.19	0.02	0.23	0.23	0.27
Ti	<0.01	<0.01	<0.01	<0.01	<0.01	<0.01	<0.01	<0.01
V	ND	ND	ND	ND	<0.01	ND	ND	<0.01
Al	0.04	0.04	0.03	0.02	<0.01	<0.01	ND	ND

All values in wt.%; ND means not detected. Other elements analyzed for included: B, Co, Nb, Sn, Ta, W, & Zr; they were either ND or only barely detectable (<0.01).

Table II - Sheet and Plate Tensile Properties

Material	yield stress	ultimate tensile strength	elongation at: max. load	failure
1.3"R.D.#	51.7 ksi (0.8)*	76.1 ksi (0.2)*	16% (0.2)*	45 % (1)*
1.3"T.D.#	51.6 (0.4)	75.2 (0.4)	16 (0.2)	41 (0.5)
0.2"R.D.	50.7 (0.4)	76.6 (0.7)	15 (2)	41 (1)
0.2"T.D.	51.4 (0.1)	76.9 (0.4)	15 (1)	32 (1)
0.09"T.D. pre-dished	53.0 (0.4)	71.2 (0.2)	15 (4)	23 (6)
0.09"R.D. Pre-dished	52.1 (0.6)	71.0 (0.6)	16 (1)	37 (3)
0.09"T.D.	52.4 (0.1)	69.6 (0.1)	16 (1)	25 (3)
0.09"R.D.	50.7 (0.5)	69.8 (0.2)	18 (0)	38 (0)
0.07"T.D.	49.4 (0.1)	70.6 (0.4)	16 (0)	34 (8)
0.07"R.D.	50.2 (1.0)	69.7 (0.4)	17 (0)	26 (6)

R.D.= rolling direction; T.D.= transverse direction.
* Standard deviation.
Two specimens each were tested for the 0.07 & 0.09" materials; three each were tested for all others.

Table II(cont'd) - Sheet and Plate Tensile Properties

True Stress/True Strain Data

$$\ln \sigma = A + B \ln \varepsilon$$

where σ, ε are true stress and true strain, respectively.

Material	A		B		Fracture Strain		$r^{\&}$	$r^{@}$
0.07"	3.89	(0.08)*	0.19	(0.02)*	0.73	(0.10)#	1.00	0.74
0.09" pre-dished	3.84	(0.12)	0.20	(0.03)	0.89	(0.11)	0.82	0.77
0.09"	3.94	(0.03)	0.18	(0.01)	0.83	(0.065)	0.81	0.71
0.2"	4.04	(0.02)	0.17	(0.01)	0.71	(0.19)	0.93	0.93
1.3"	3.95	(0.05)	0.20	(0.01)	1.10	(0.14)	1.26	1.08

*90% confidence limit deviation
#standard deviation
& = "r" value at max. load
@ = "r" value from ratio of slopes

Table III - Weld Tensile Properties

Weld Identification	Transverse Strength Yield	Maximum	Fracture Location
0.07" to 0.07" with 1" x 2" backing bar	3370 lbs/in (40)#	4700 lbs/in (15)#	base metal
	3540 (360)	5260 (670)	*fusion line
0.07" to bottom corner	3590 (20)	4860 (20)	base metal
	3100 (70)	5140 (50)	*fusion line
Penetration (1.3" mat'l reduced to 0.5") to 0.2" insert plate	10300 (60)	15300 (100)	base metal
	11100 (140)	18400 (420)	*fusion line
Penetration dome (0.2") to Penetration (1.3" mat'l reduced to 0.5")	--	11000 (3550)	2 at fusion line, 1 in base metal
Bottom corner to 0.07" bottom with 1" x 2" backing bar	3740 (730)	4920 (120)	base metal
	3980 (40)	5440 (250)	*fusion line
Stud weld to 0.07" sheet	--	926 (110)	pulled nuggets
Stud weld to 0.09" sheet	--	1245 (375)	"
Stud weld to 0.2" sheet	--	1125 (639)	2 broke in stud, 2 pulled small nuggets, 2 broke off in handling (not counted for average and sd).

#Standard deviation
*Reduced in width at fusion zone to force failure into weld.

Table III - Weld Tensile Properties (cont'd)

0.07" sheet to 0.07", 0.09" sheet or 0.2" sheet	3360 lb/in (140)	4590 lb/in (80)	base metal 18 % (sd1%) elongation to failure in 2" gauge length for 0.07" mat'l.
0.09" to 0.09" sheet	4280 lb/in (120)	5840 lb/in (40)	base metal 16% (sd 2%) elongation to failure in 2" gauge length.

All Weld Metal Longitudinal Tensile Properties

	yield stress	ultimate tensile strength	elongation at: max load	failure
0.07" to 0.07" 0.09" to 0.09" flat and vertical welding positions	67.6 ksi (2.6)	84.9 ksi (3.7)	8% (1)	11% (2)
0.07" to 0.07" 0.07" to 0.09" horizontal welding position.	63.8 (1.8)	79.8 (3.0)	8 (0)	10 (0)
0.07" to 0.2" vertical welding position.	85.5 (2.9)	104.7 (5.3)	*	*
0.07" to 0.2" horizontal welding position.	74.8 (3.9)	95.9 (4.4)	5 +	7 +

*All samples broke outside extensometer gauge length.
+Only one sample did not break outside extensometer gauge length.

Table IV - Rebar Tensile Properties

Material	Yield Load	Maximum Load	Elongation at: Max. load	Failure
6 mm	3340 lb	4330	10%	*
	(60)#	(70)#	(2)#	*
No.3	7160	11020	11	*
	(130)	(190)	(1)	*
No.4	12730	20440	11	21%
	(280)	(380)	(1)	(2)
No.5	21240	32850	11	22
	(310)	(300)	(1)	(0)

Standard deviation.

*All specimens broke outside the extensometer gauge length. Four specimens were tested for each size except No. 4, where 20 were tested

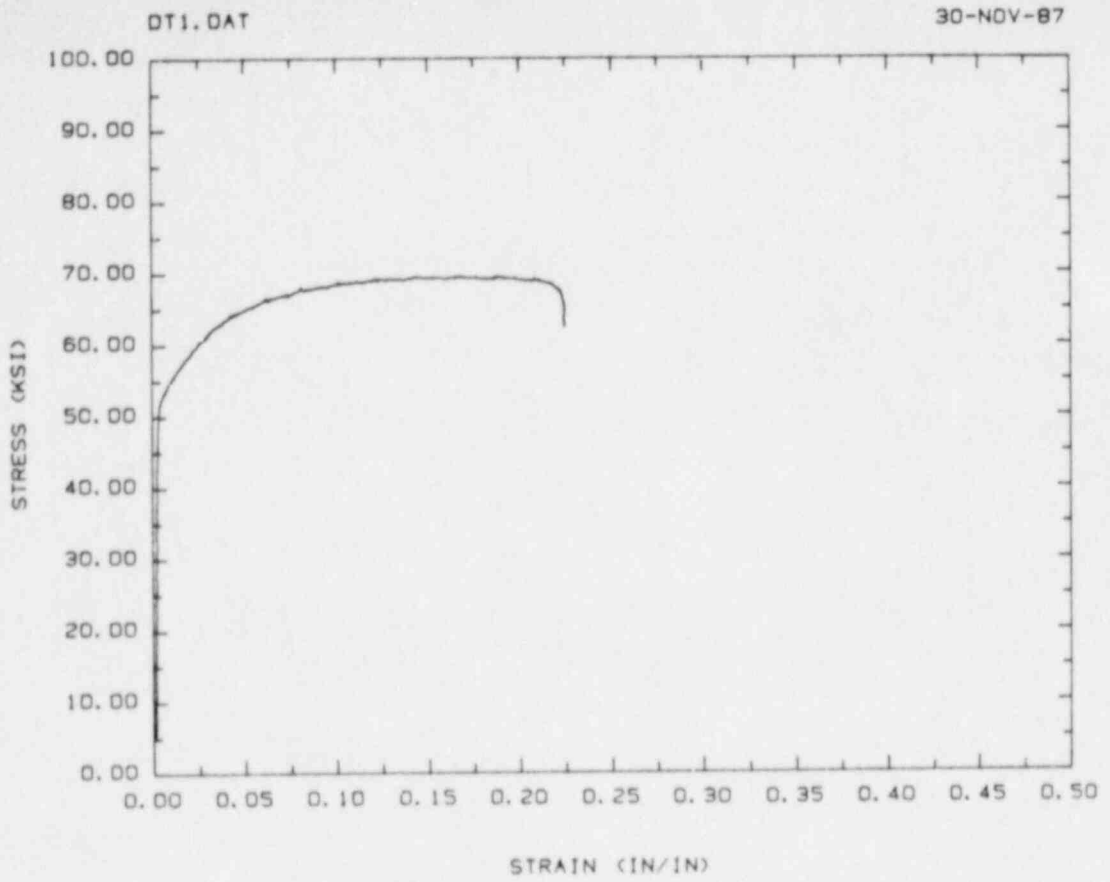

Figure 1 Engineering stress/strain curve for dome material

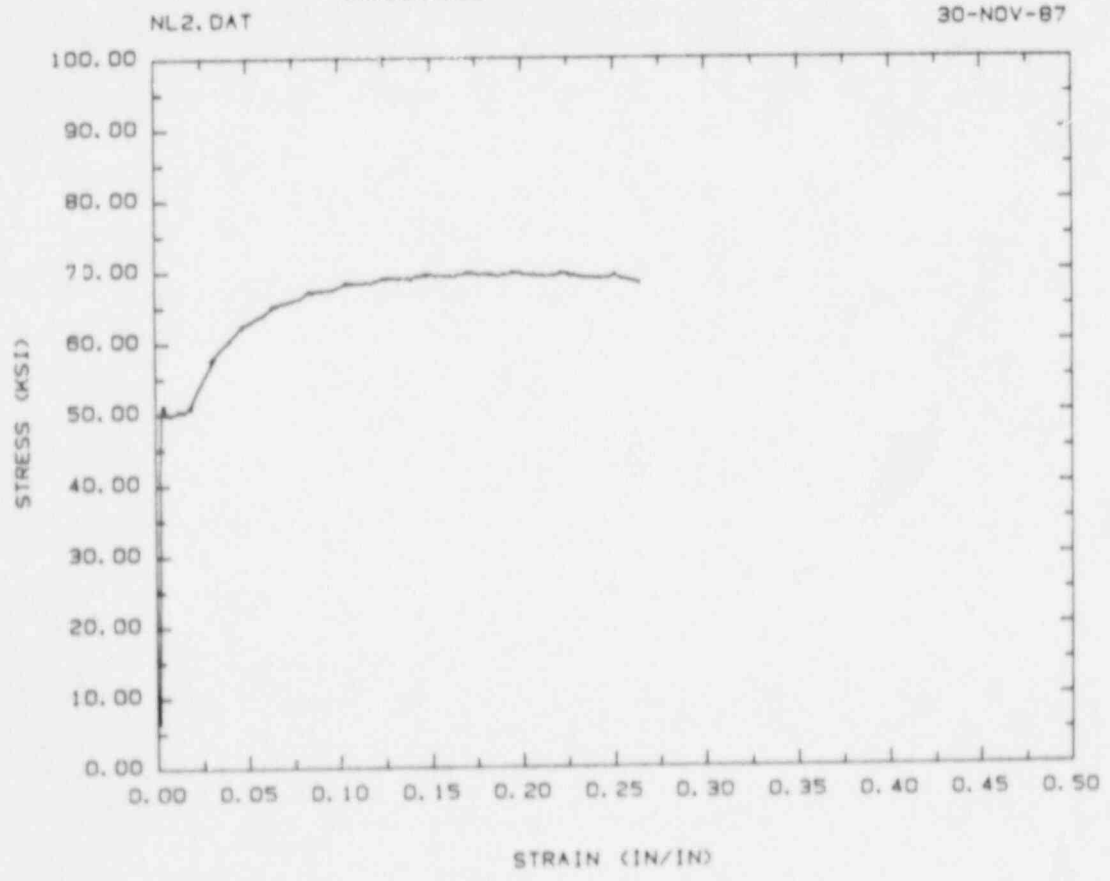

Figure 2 Engineering stress/strain curve for cylinder material

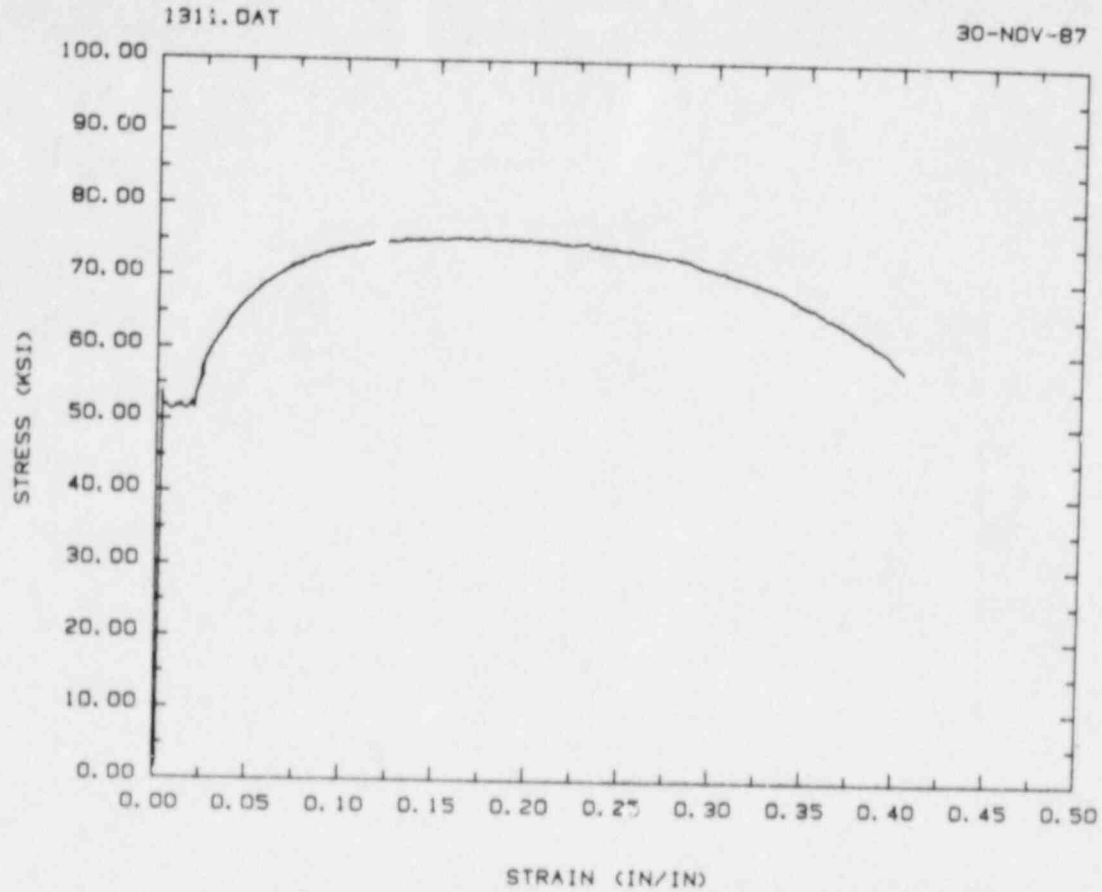

Figure 3 Engineering stress/strain curve for penetration sleeve material

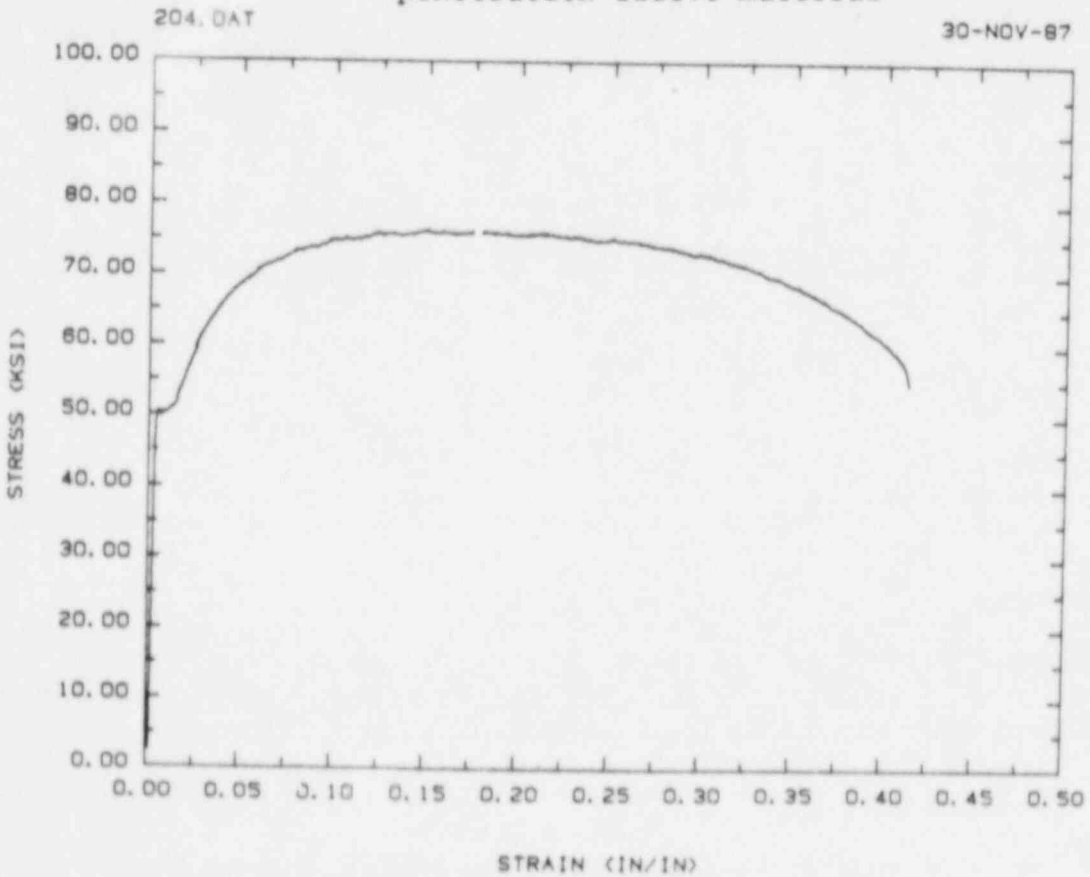

Figure 4 Engineering stress/strain curve for insert plate material

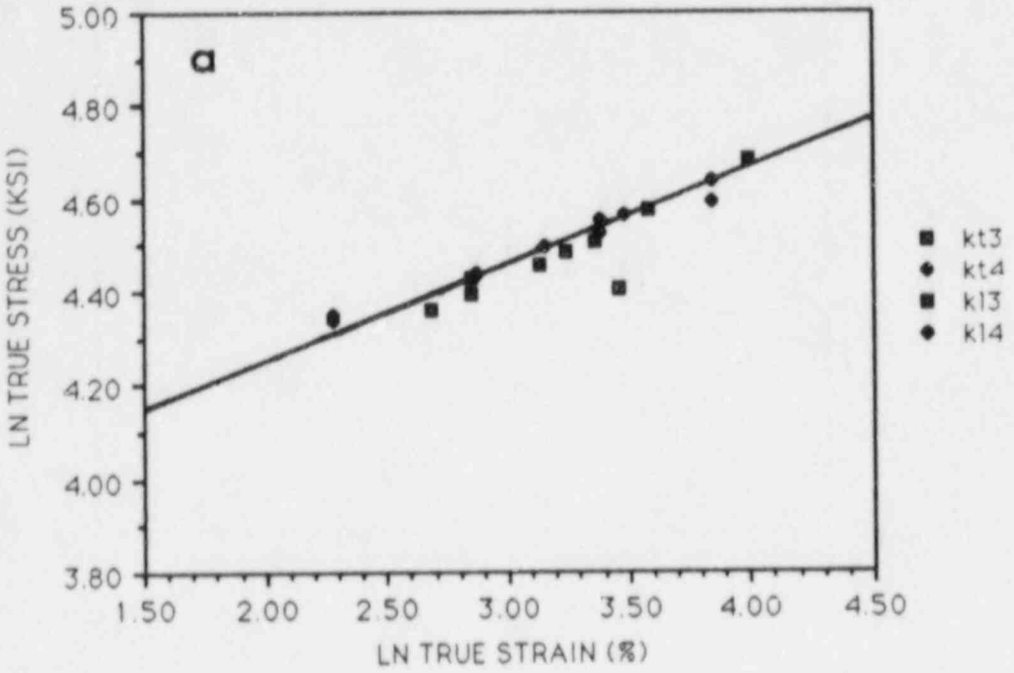

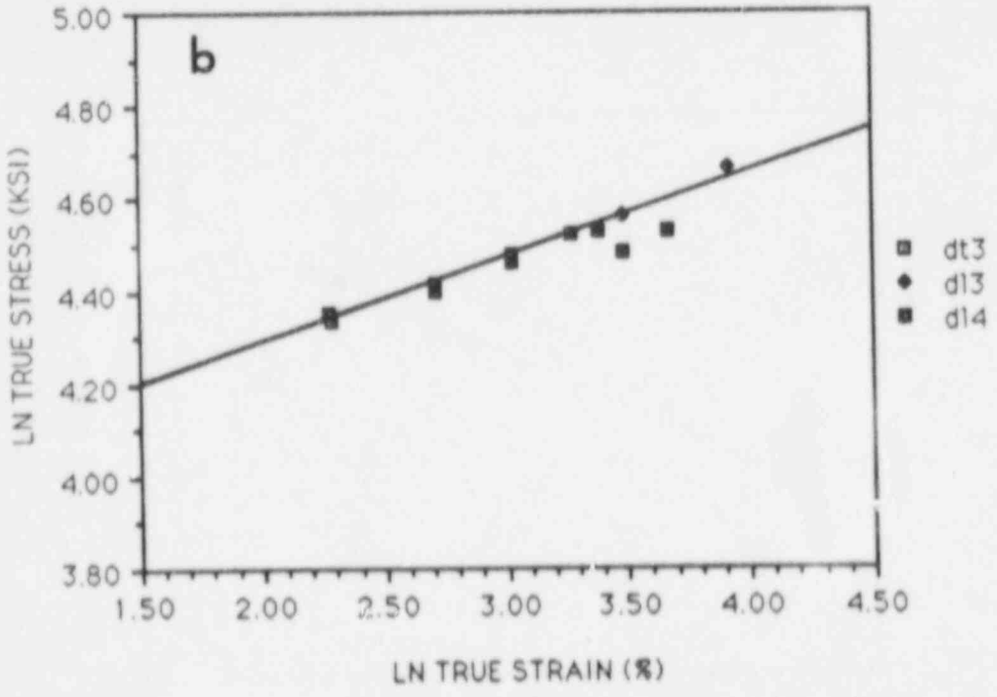

Figure 5 True stress/strain data for dome material a) pre-dished condition, b) post- dished condition

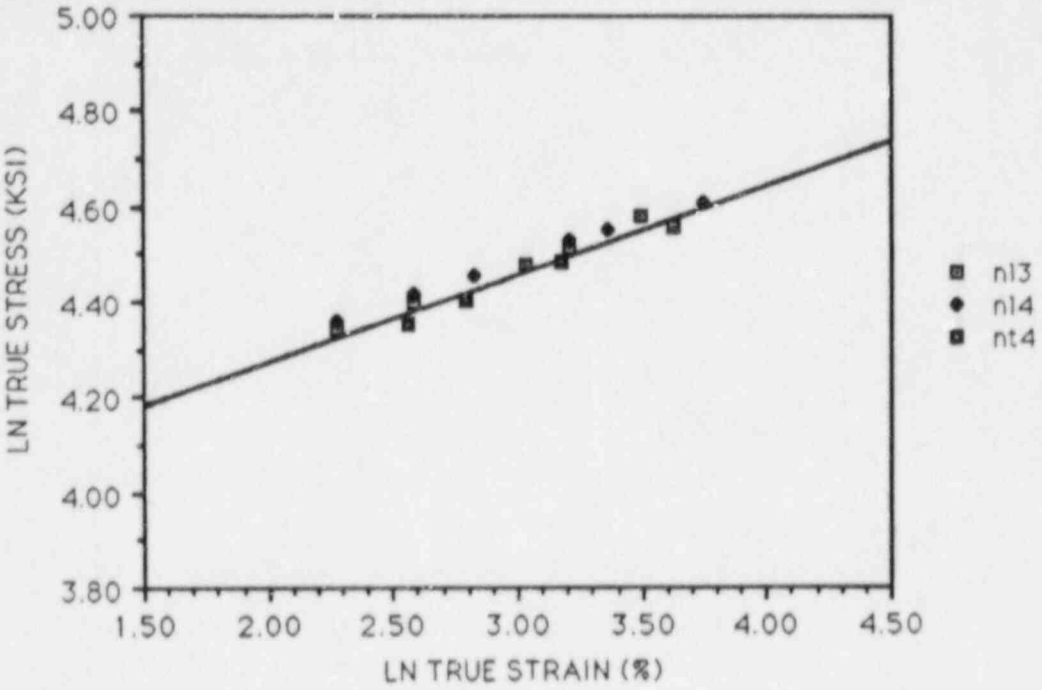

Figure 6 True stress/strain data for cylinder material

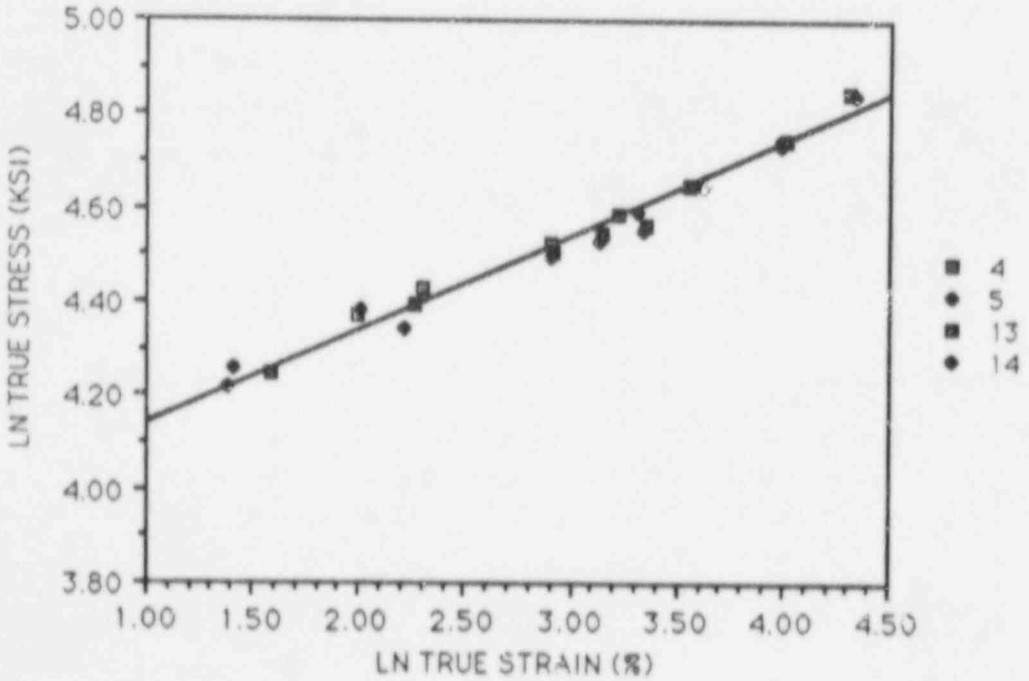

Figure 7 True stress/strain data for penetration sleeve material

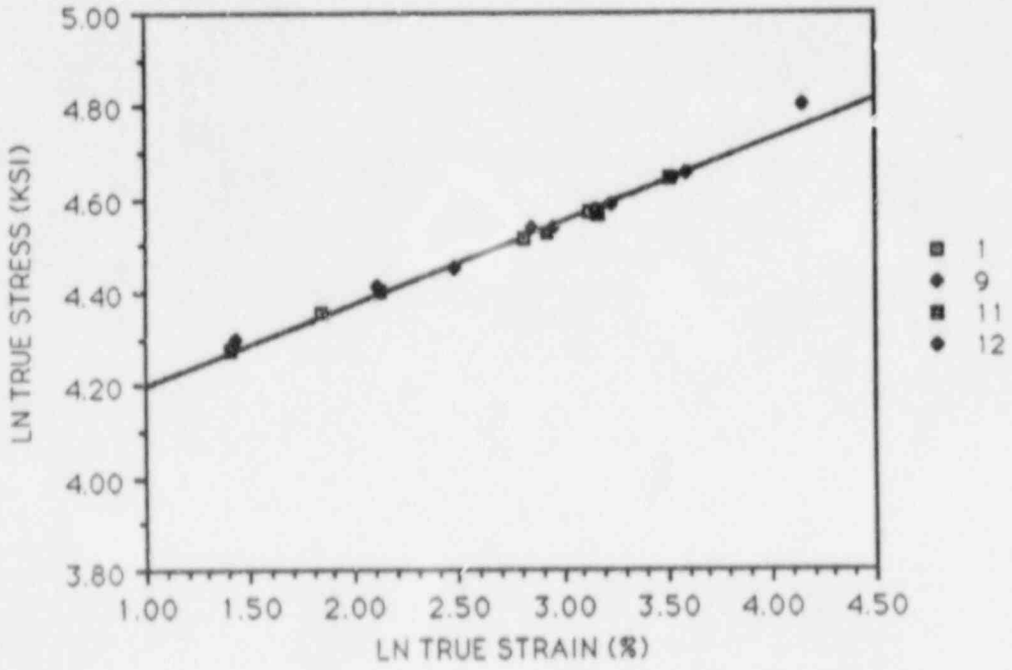

Figure 8 True stress/strain data for insert plate material

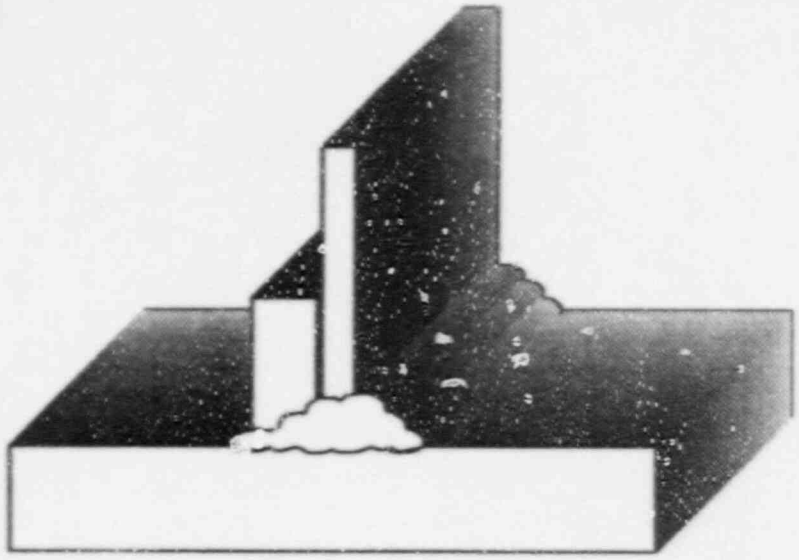

a) Penetration sleeve (1.3" reduced to 0.5") to insert plate (0.2"), with backup bar.

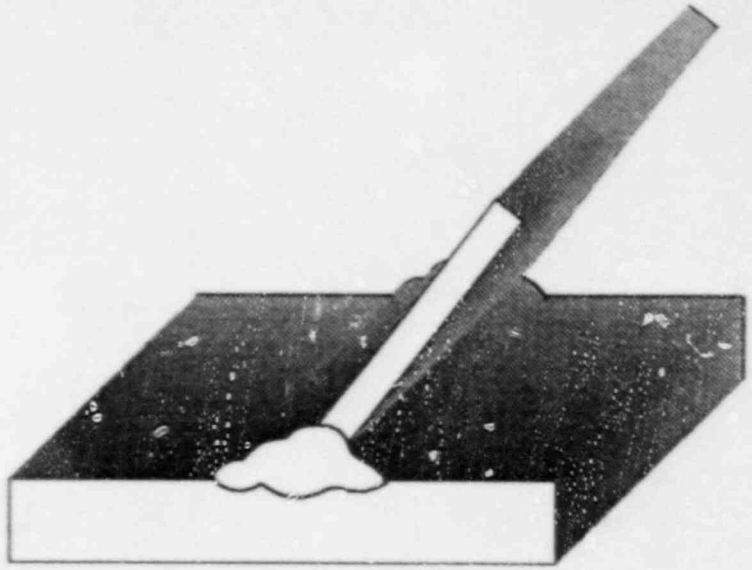

b) Equipment hatch dome (0.2") to tension ring.

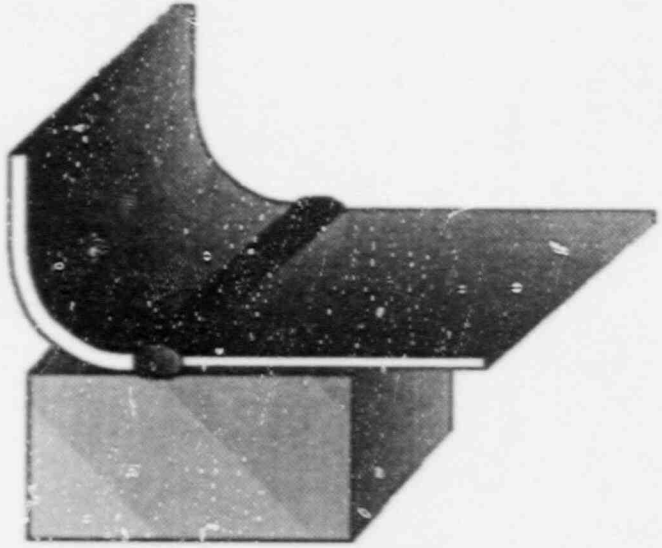

c) Bottom corner to 0.07" bottom with 1" x 2" backing bar (does not illustrate 0.07" cylinder to bottom corner weld).

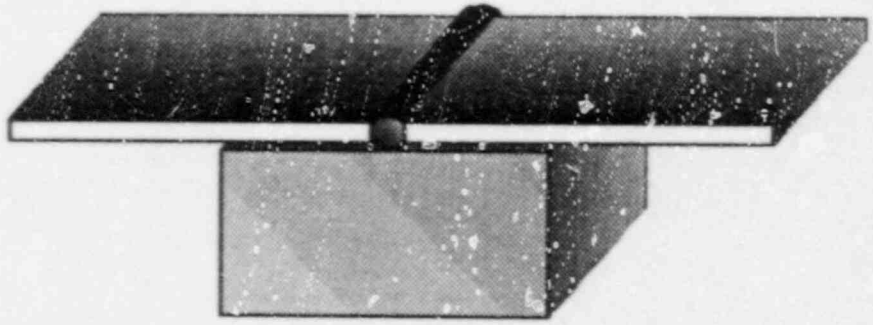

d) 0.07" bottom to 0.07" bottom with 1" x 2" backing bar.

Figure 9 Additional weld specimen geometries.

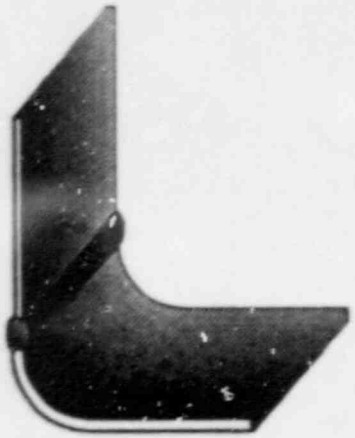

e) 0.07" cylinder to bottom corner.

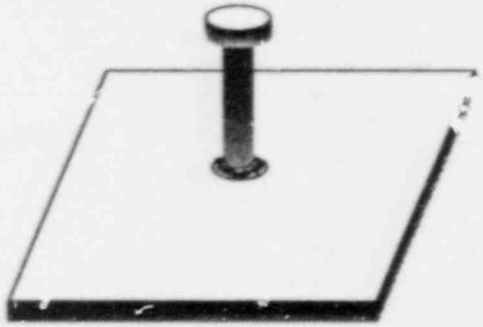

f) Stud welds, 1/8" shaft to plates 0.07" thick, 0.09" thick and 0.2" thick.

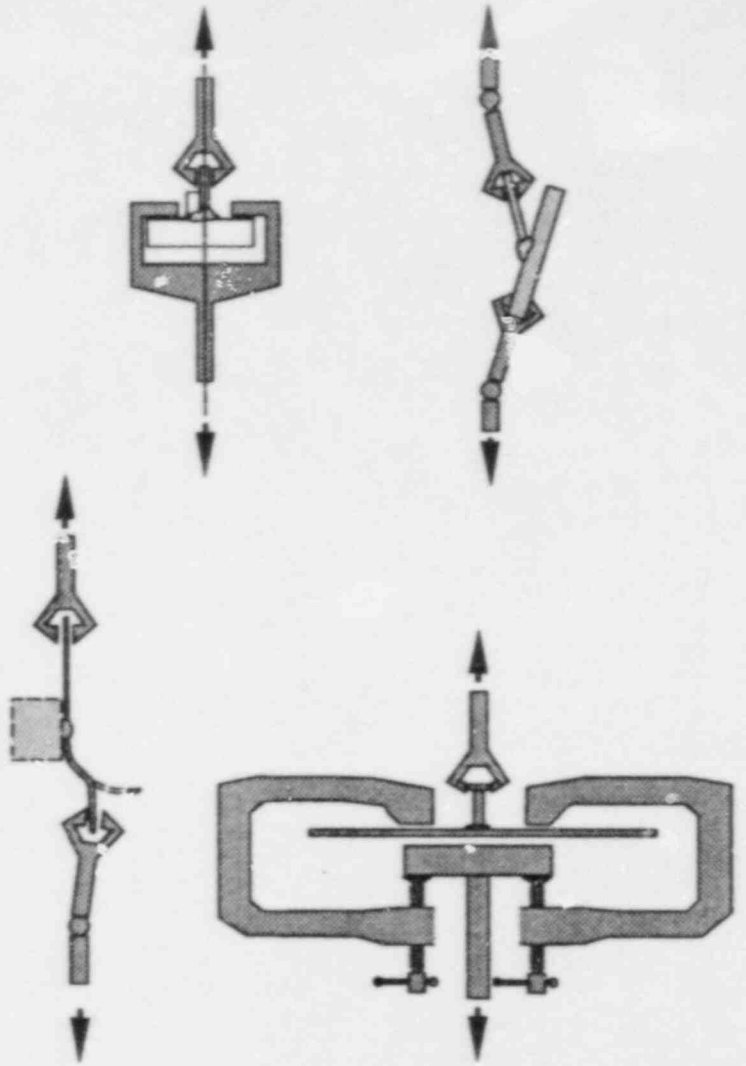

g) Details of loading geometries.

Figure 9 Additional weld specimen geometries.

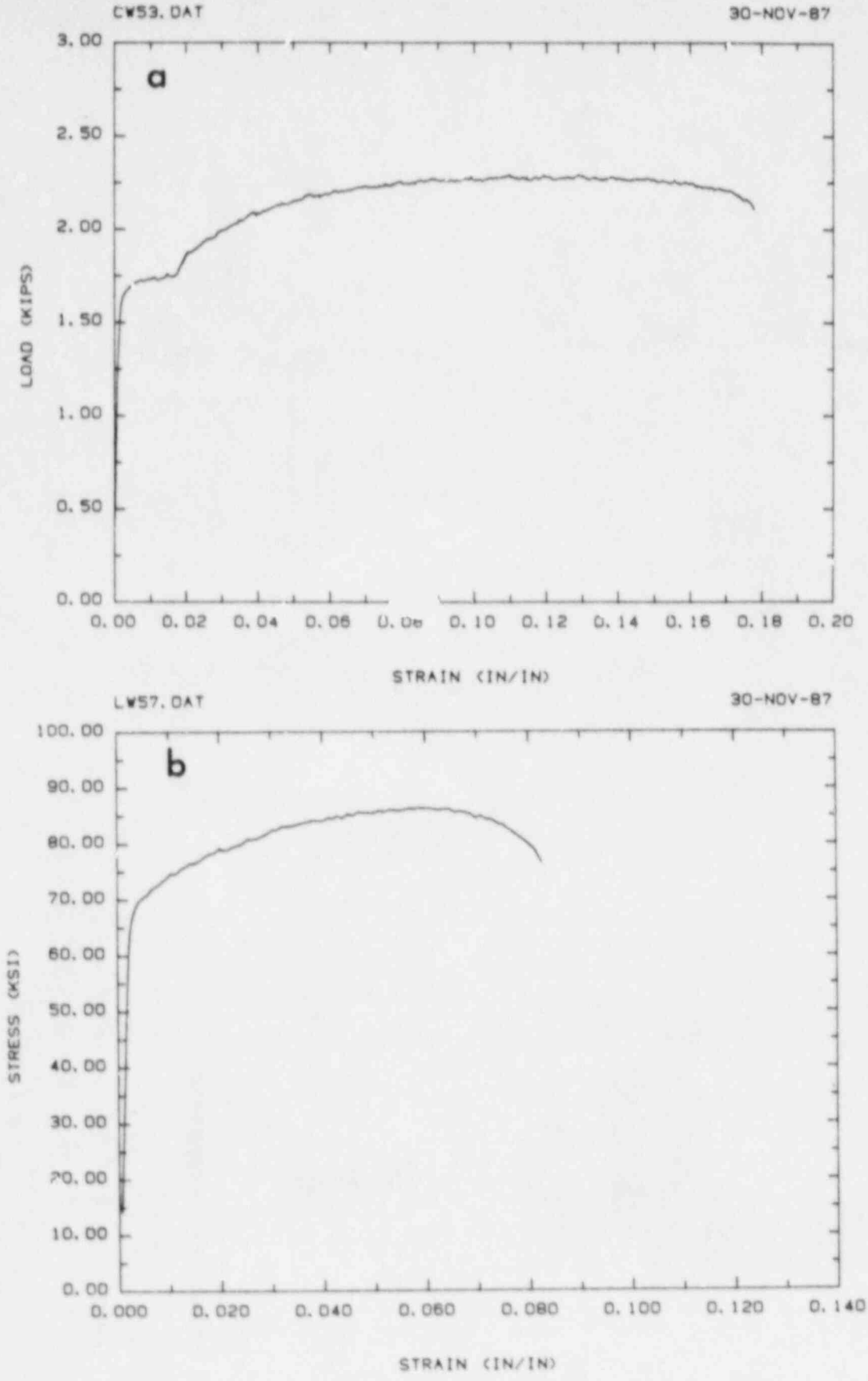

Figure 10 a) Cross-weld load/engineering strain curve and b) all weld metal engineering stress/strain curve for cylinder/cylinder specimen

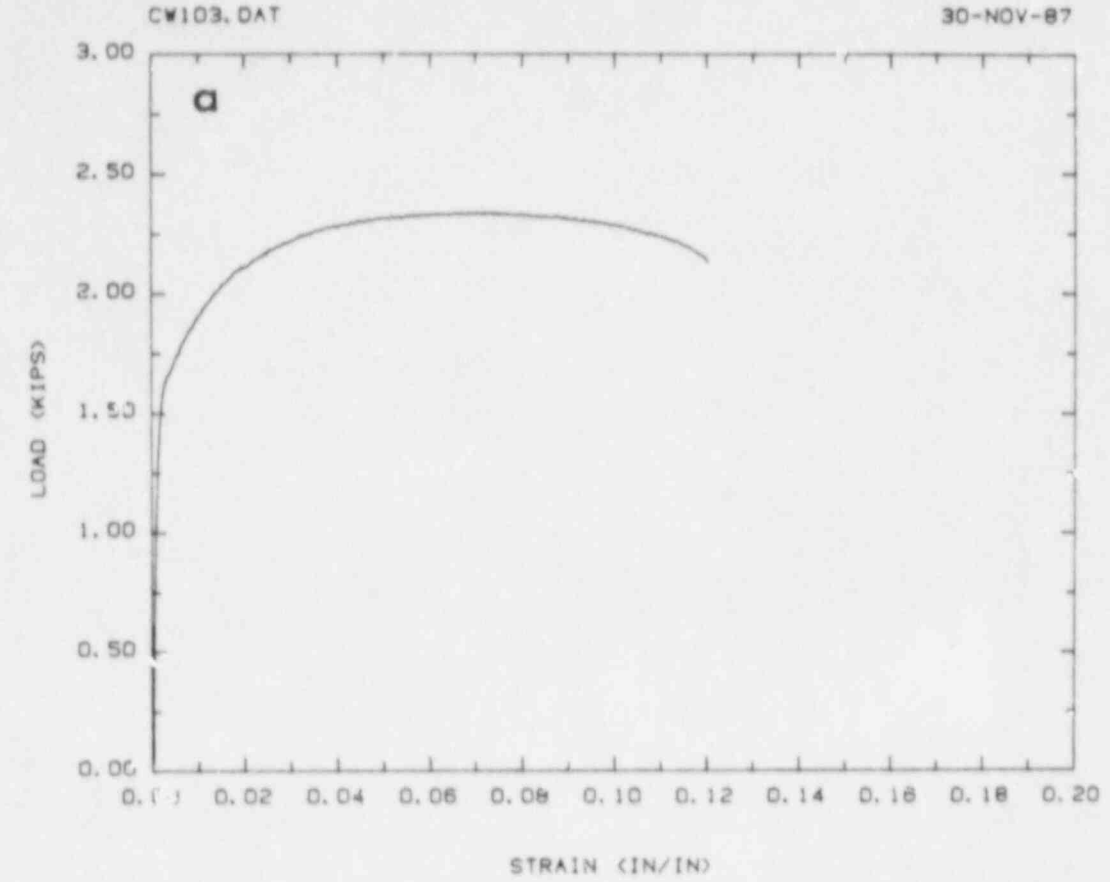

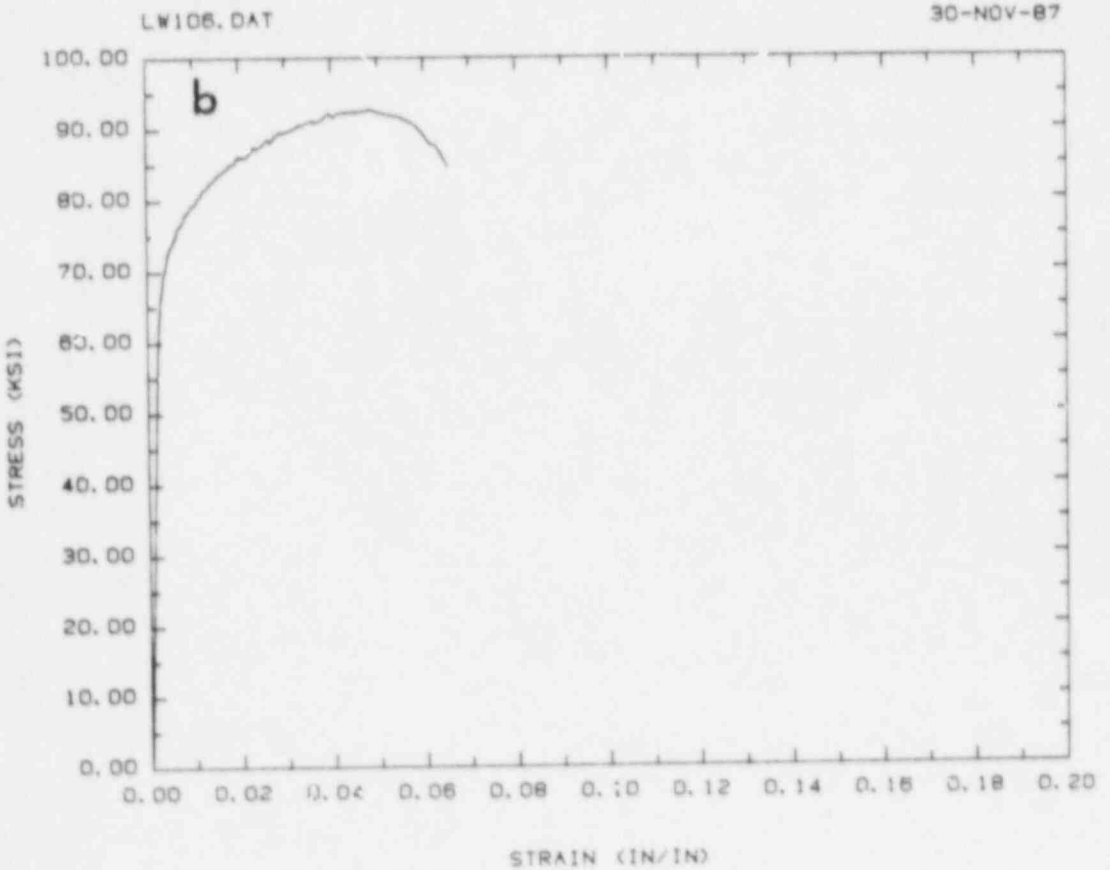

Figure 11 a) Cross-weld load/engineering strain curve and b) all weld metal engineering stress/strain curve for cylinder/insert plate specimen

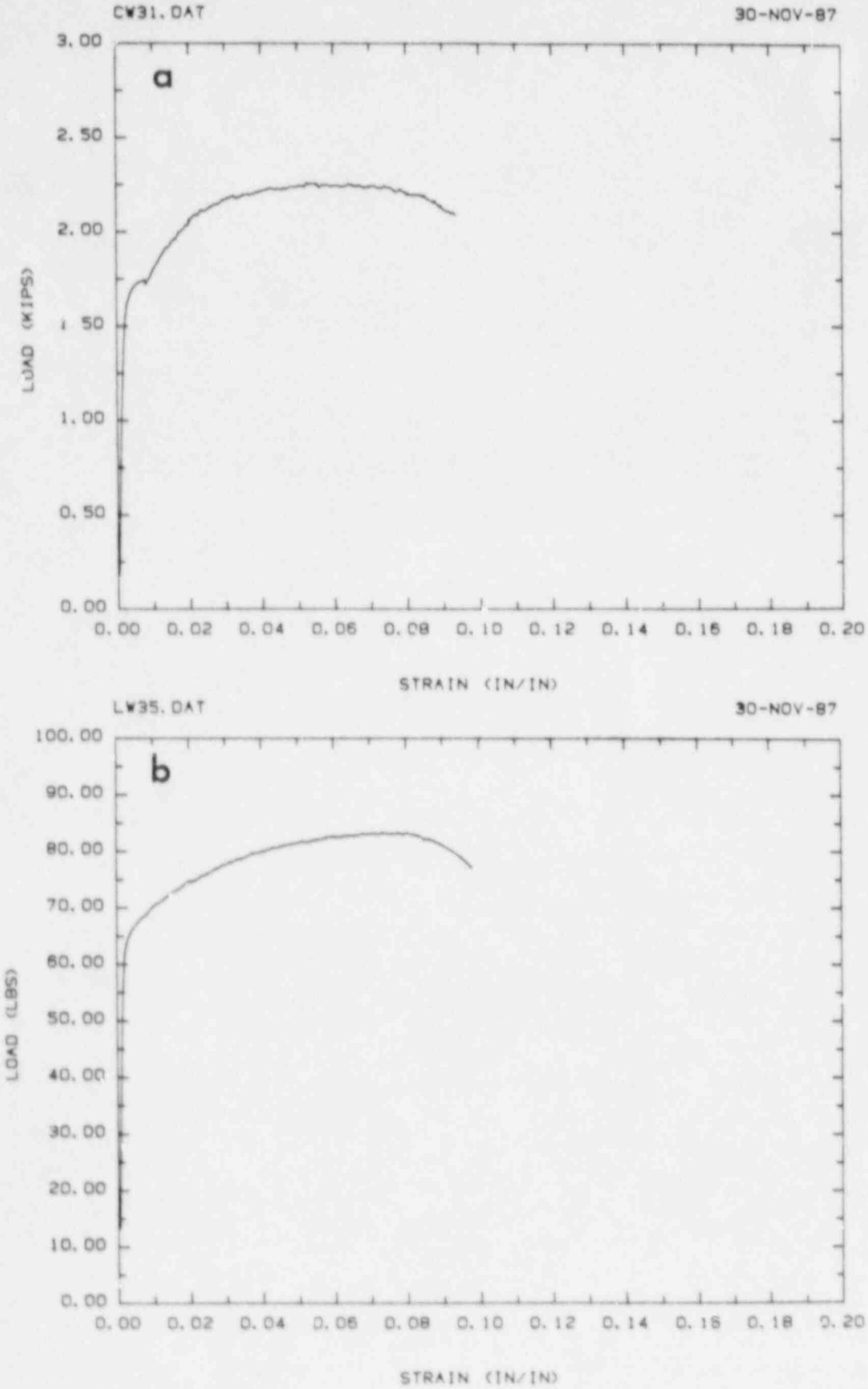

Figure 12 a) Cross-weld load/engineering strain curve and b) all weld metal engineering stress/strain curve for cylinder/dome specimen

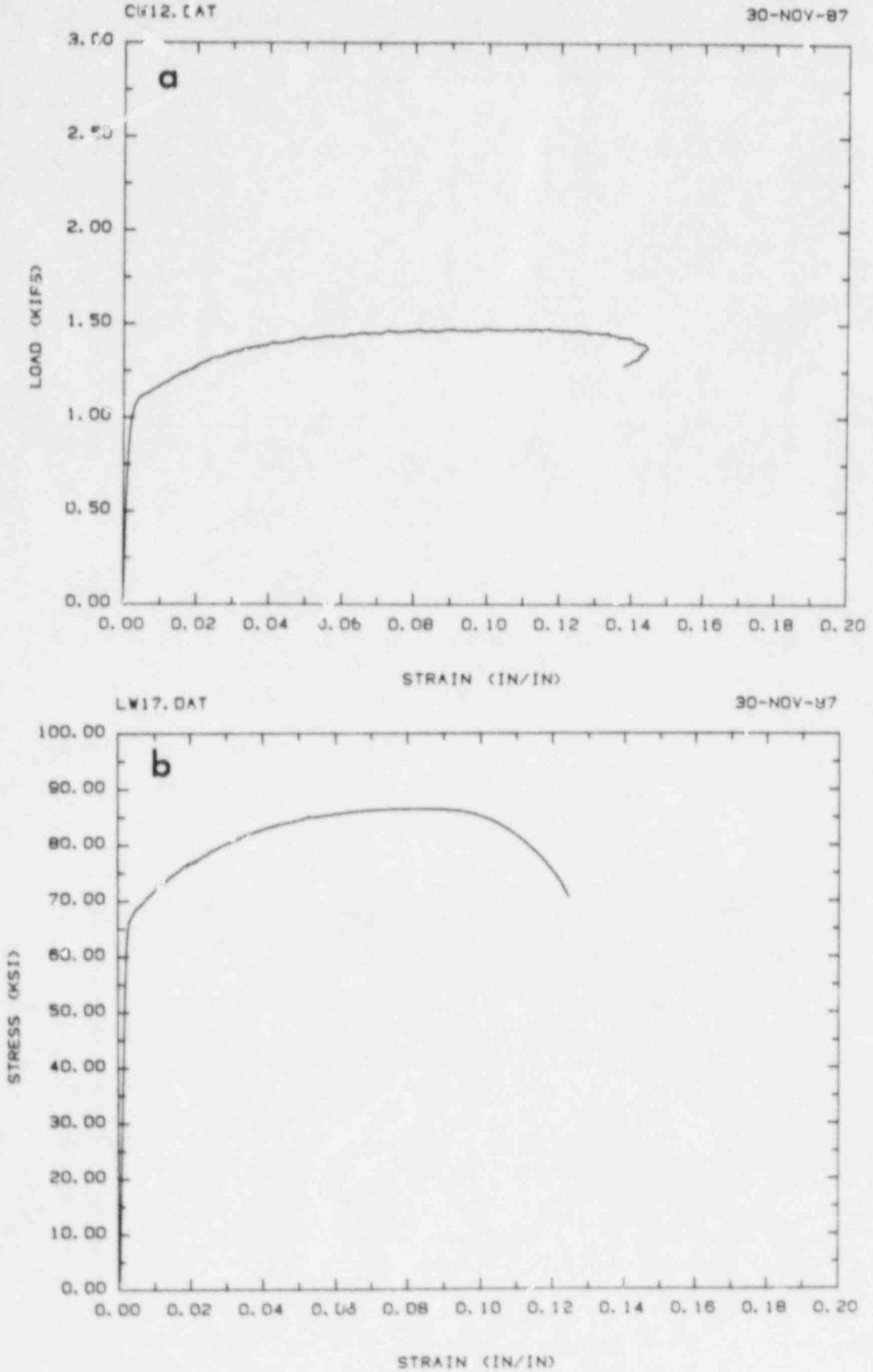

Figure 13 a) Cross-weld load/engineering strain curve and b) all weld metal engineering stress/strain curve for dome/dome specimen

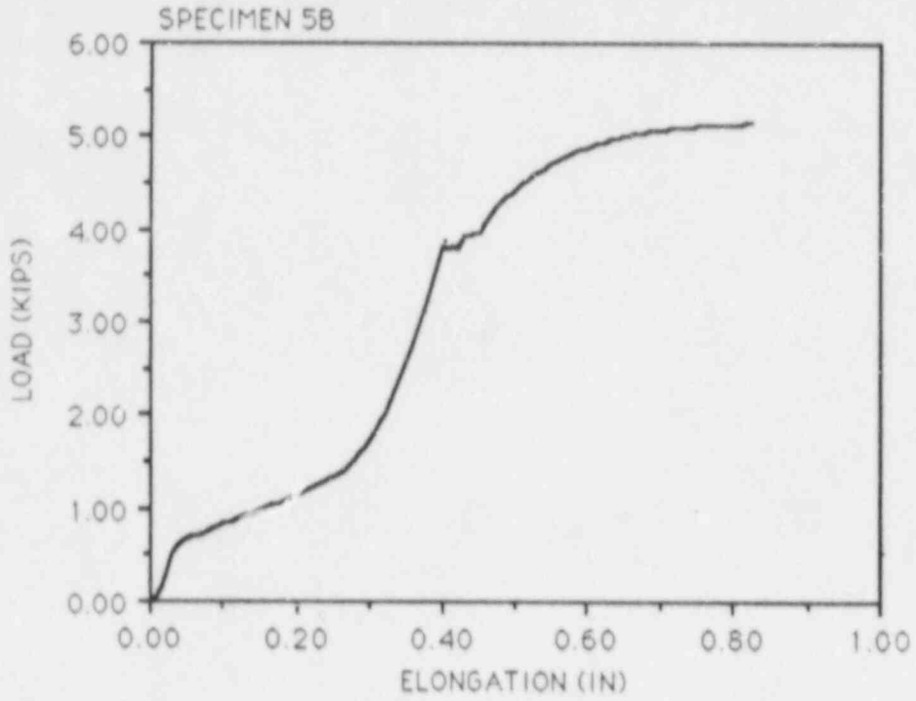

Figure 14 Cross-weld load/elongation curve for cylinder/bottom corner specimen

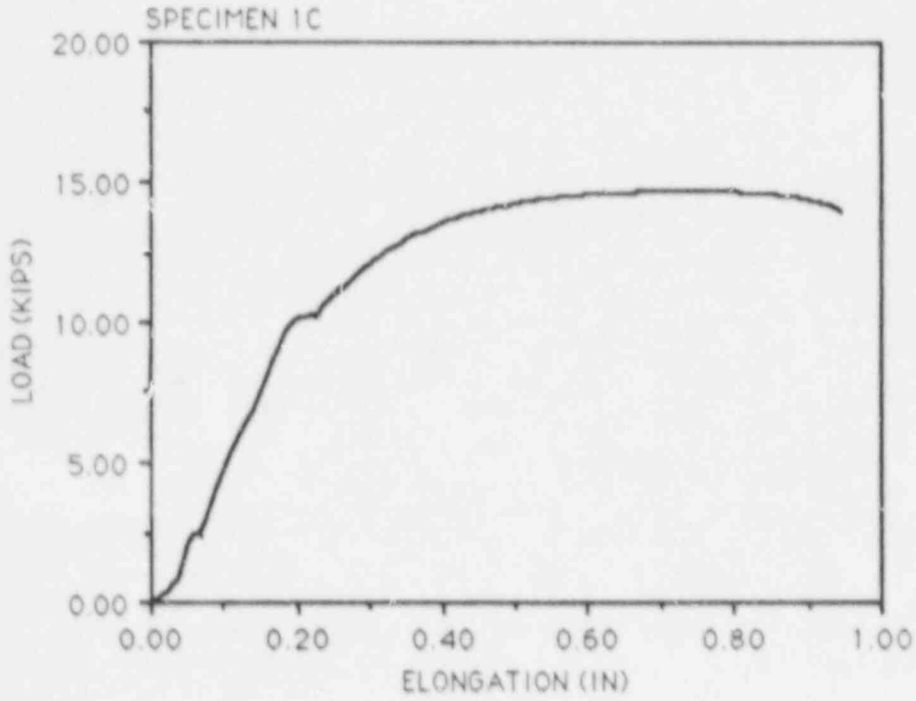

Figure 15 Cross-weld load/elongation curve for penetration sleeve/insert plate specimen

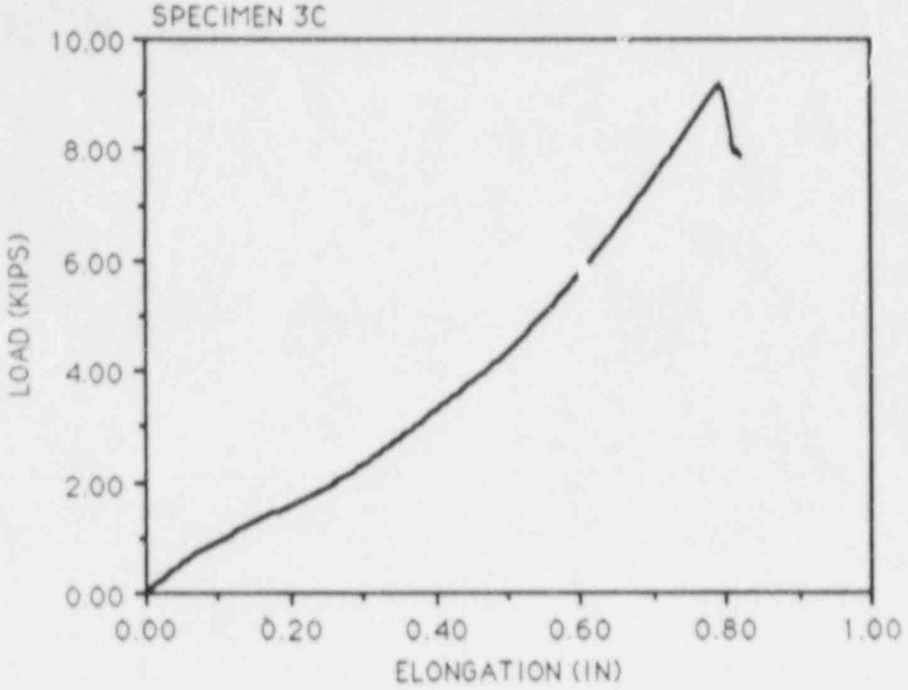

Figure 16 Cross-weld load/elongation curve for equipment hatch dome to tension ring specimen

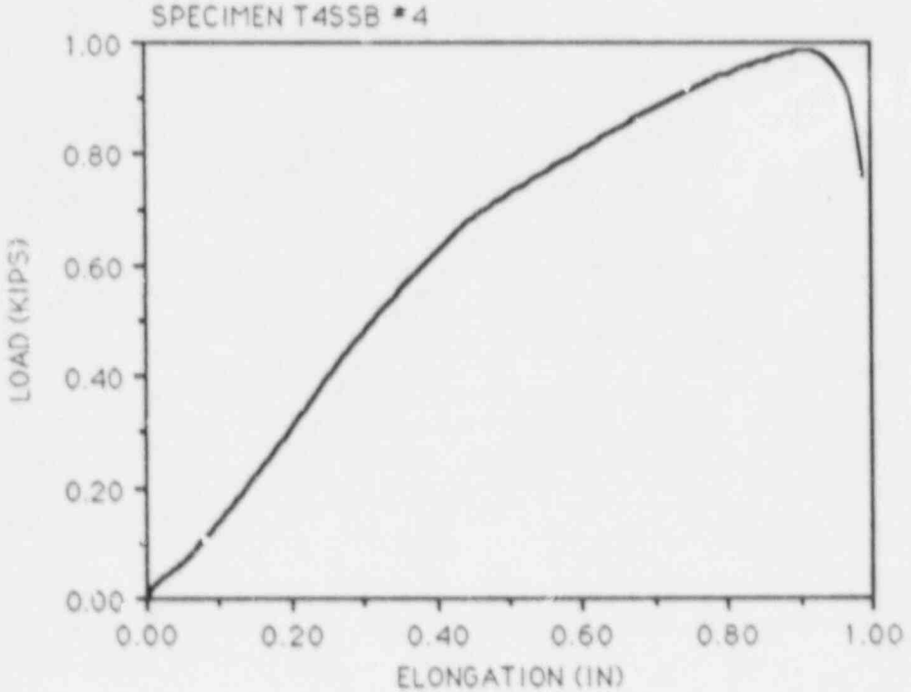

Figure 17 Load/elongation curve for stud to cylinder weld

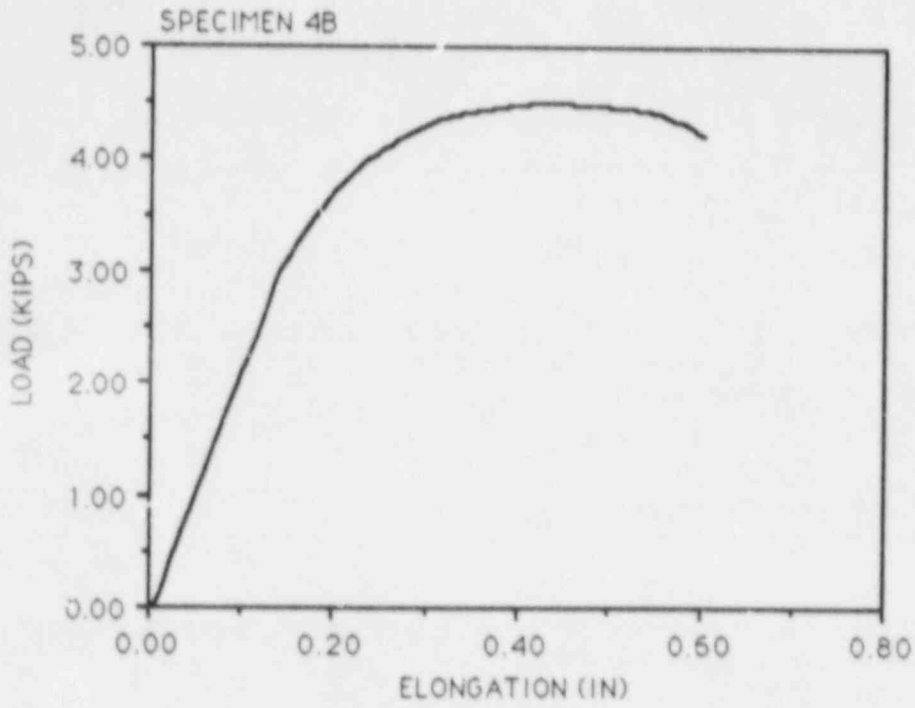

Figure 18 Cross-weld load/elongation curve for bottom corner to bottom with backing bar

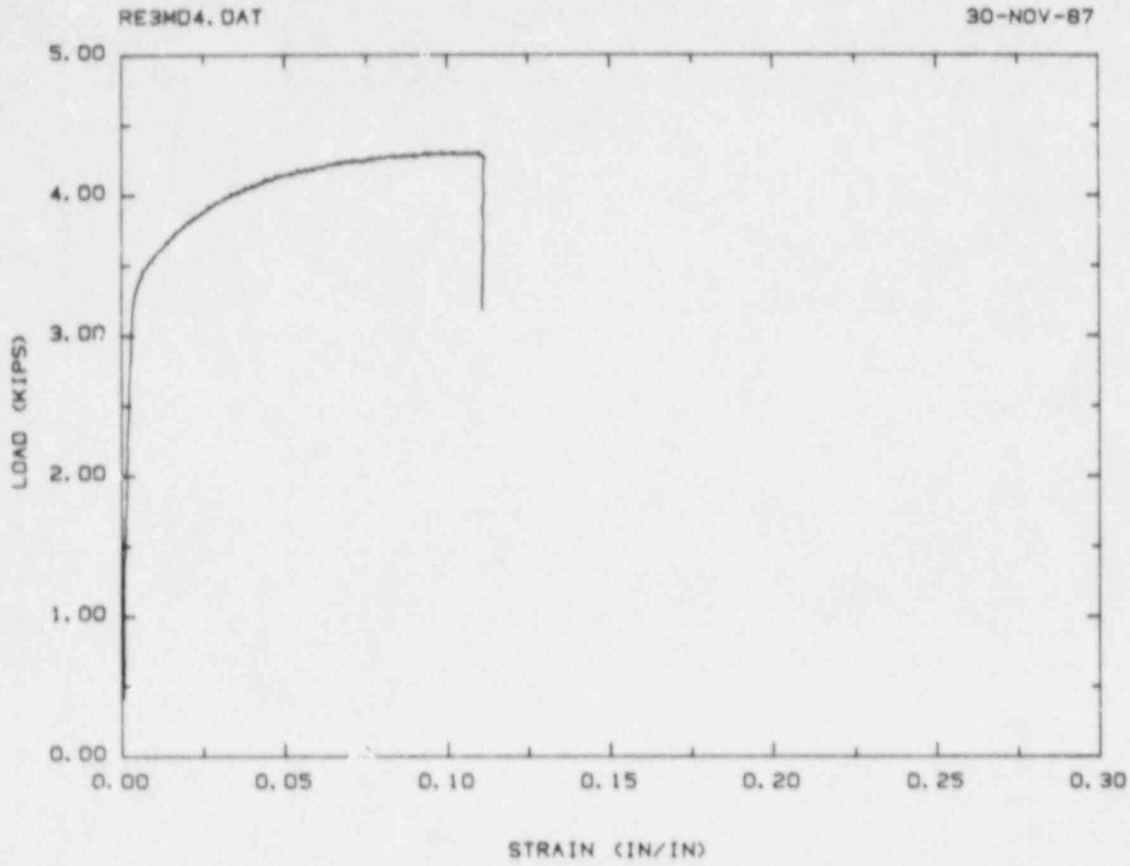

Figure 19 6 mm rebar load/engineering strain curve

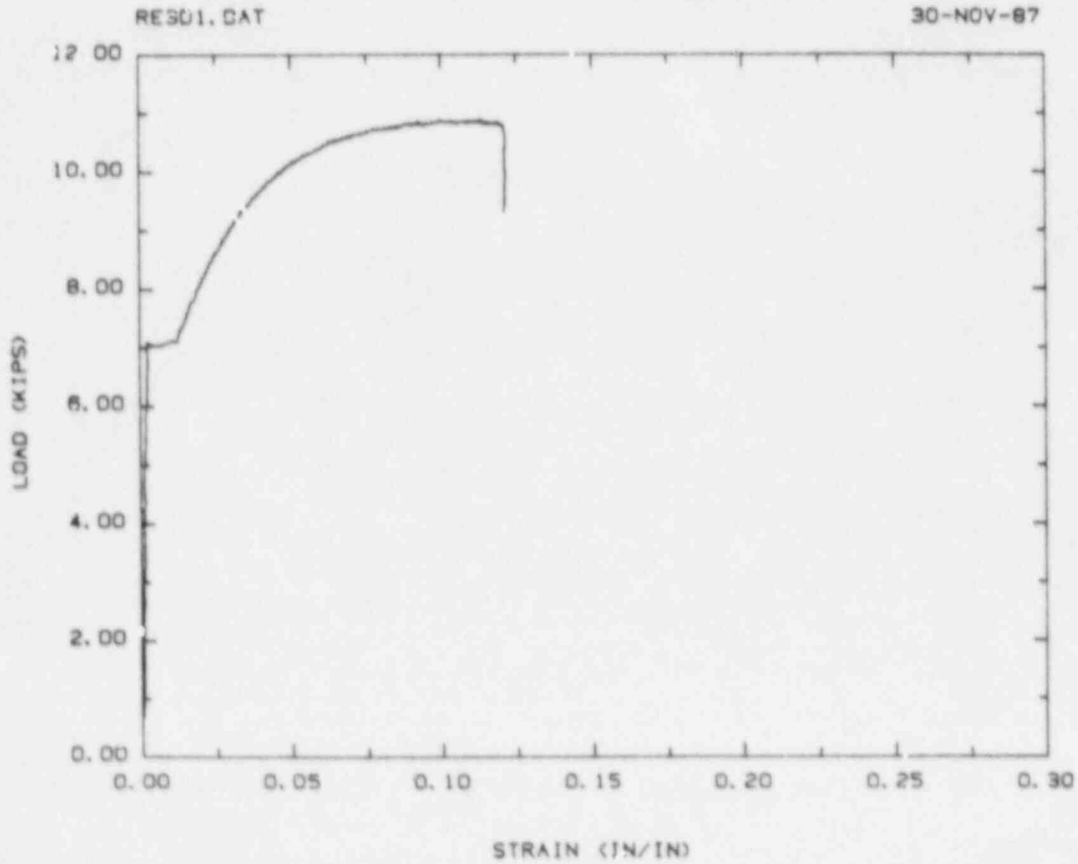

Figure 20 #3 rebar load/engineering strain curve

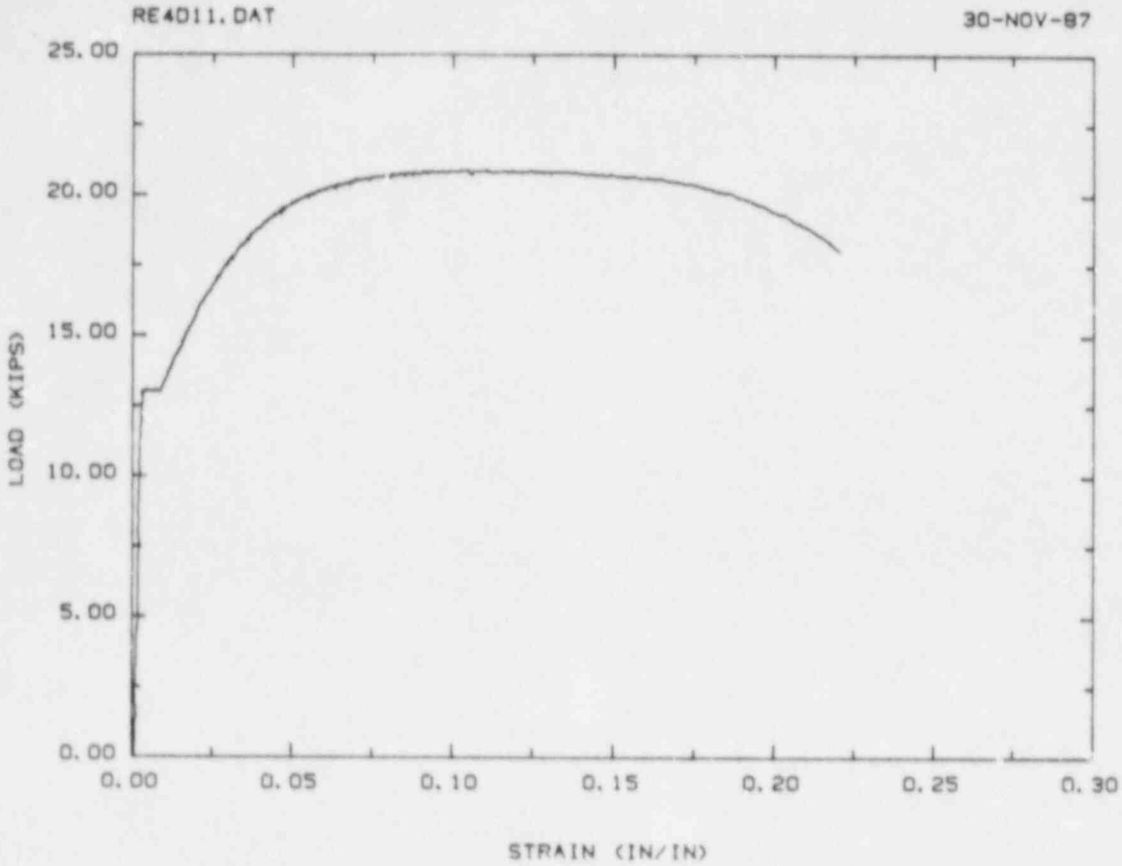

Figure 21 #4 rebar load/engineering strain curve

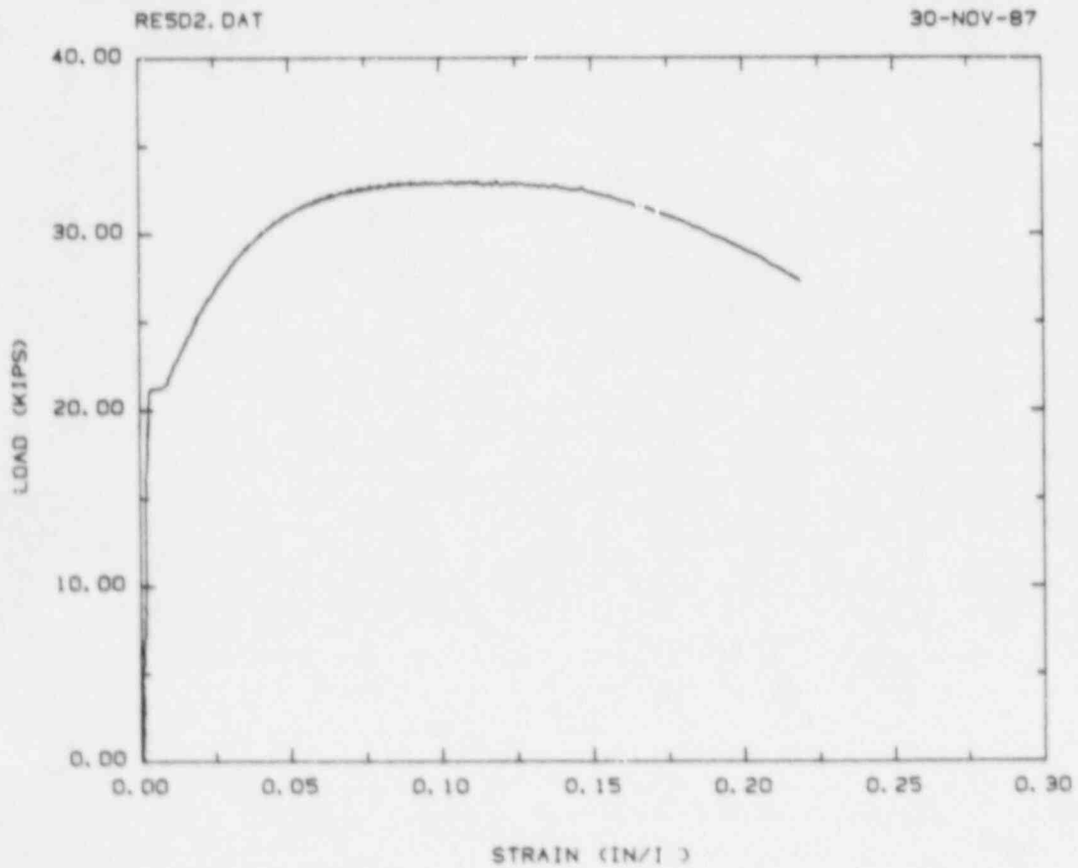

Figure 22 #5 rebar load/engineering strain curve

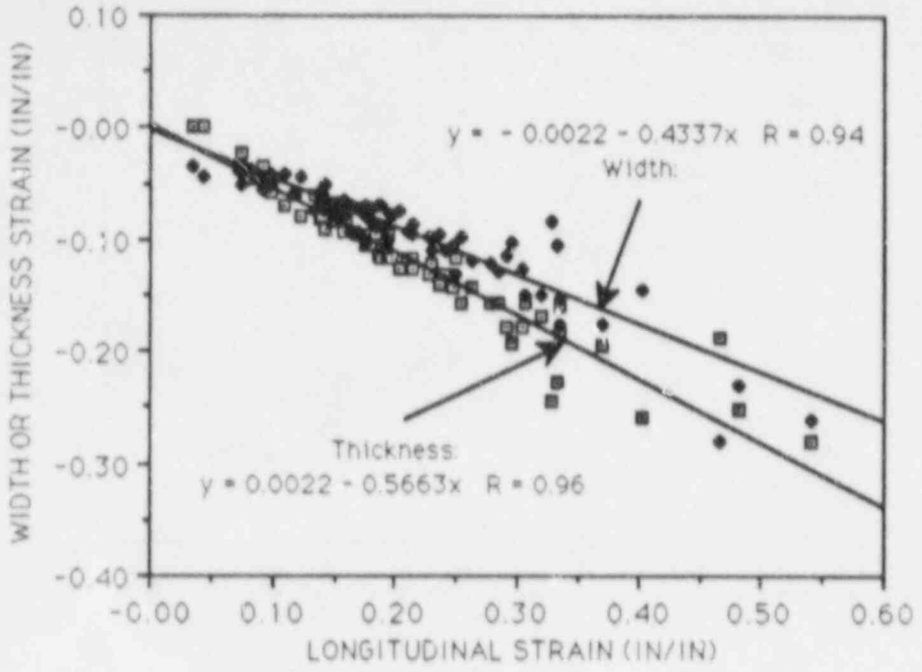

Figure 23 True width and thickness strain vs.true longitudinal strain for done material

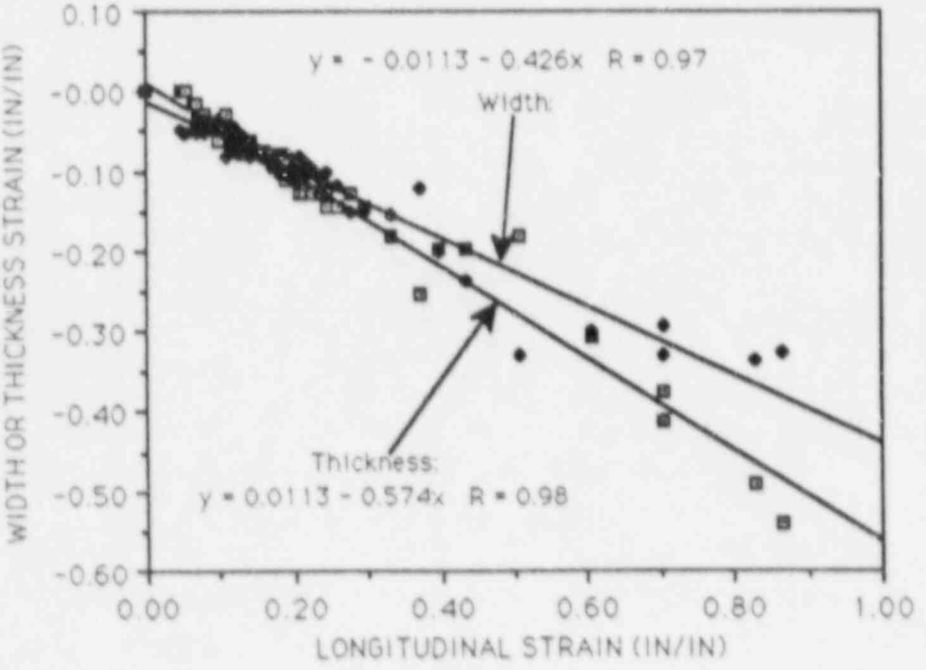

Figure 24 True width and thickness strain vs. true longitudinal strain for cylinder material

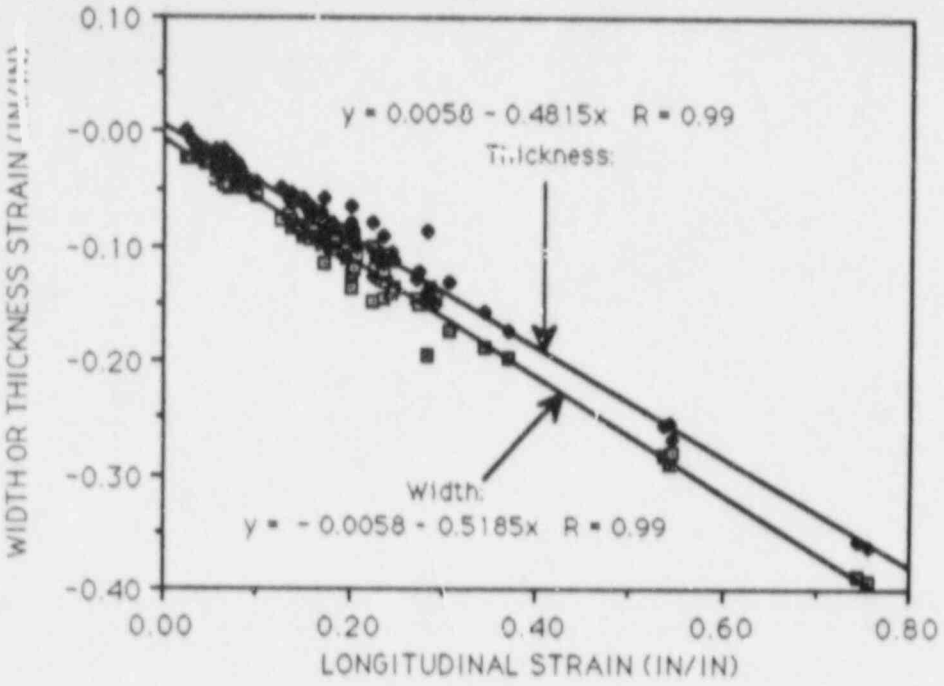

Figure 25 True width and thickness strain vs. true longitudinal strain for penetration sleeve material

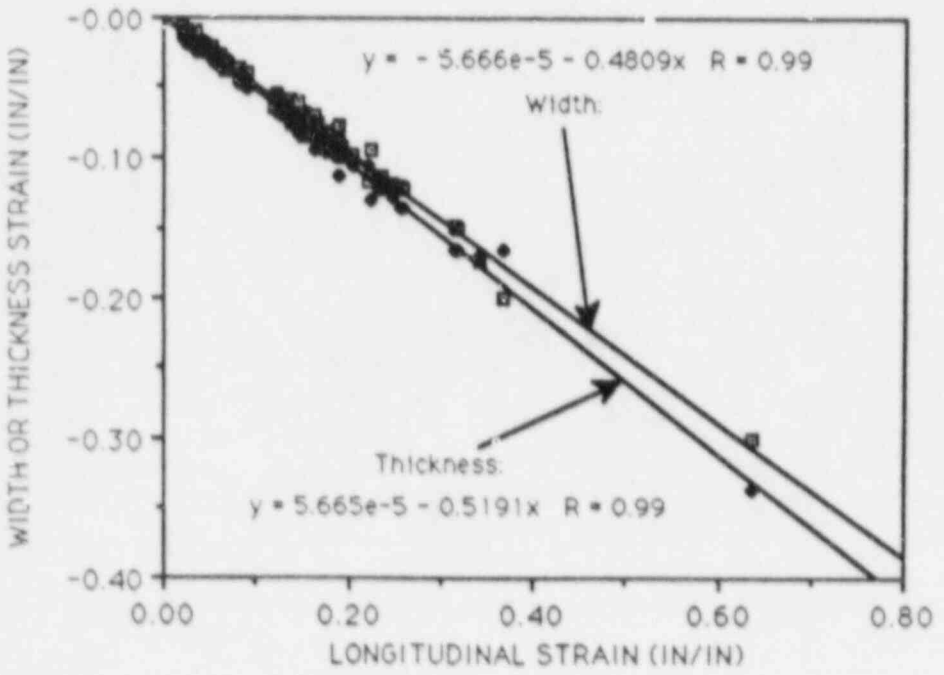

Figure 26 True width and thickness strain vs. true longitudinal strain for insert plate material

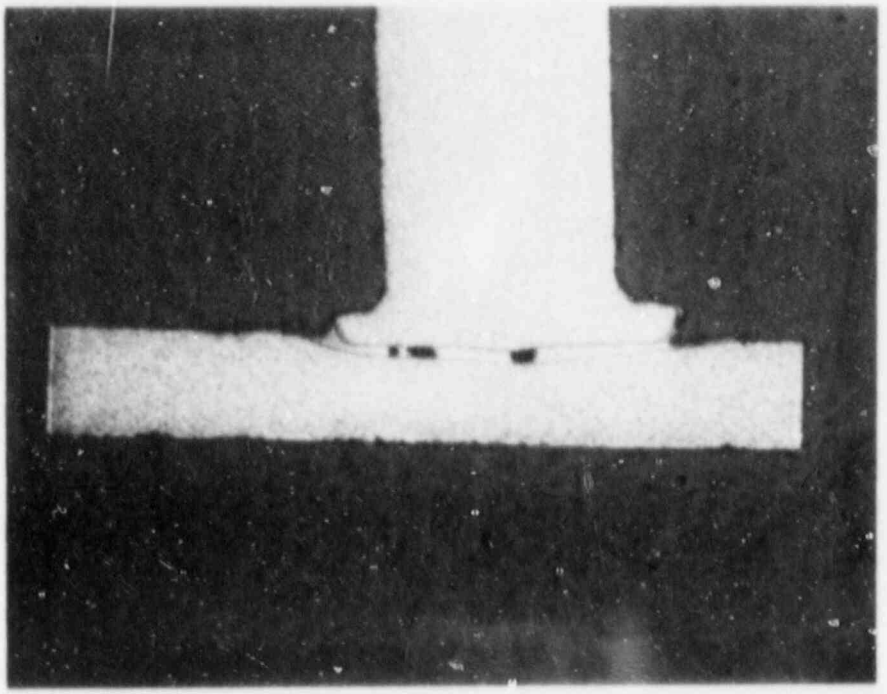

Figure 27 Cross-section of stud weld to cylinder material (8.5x)

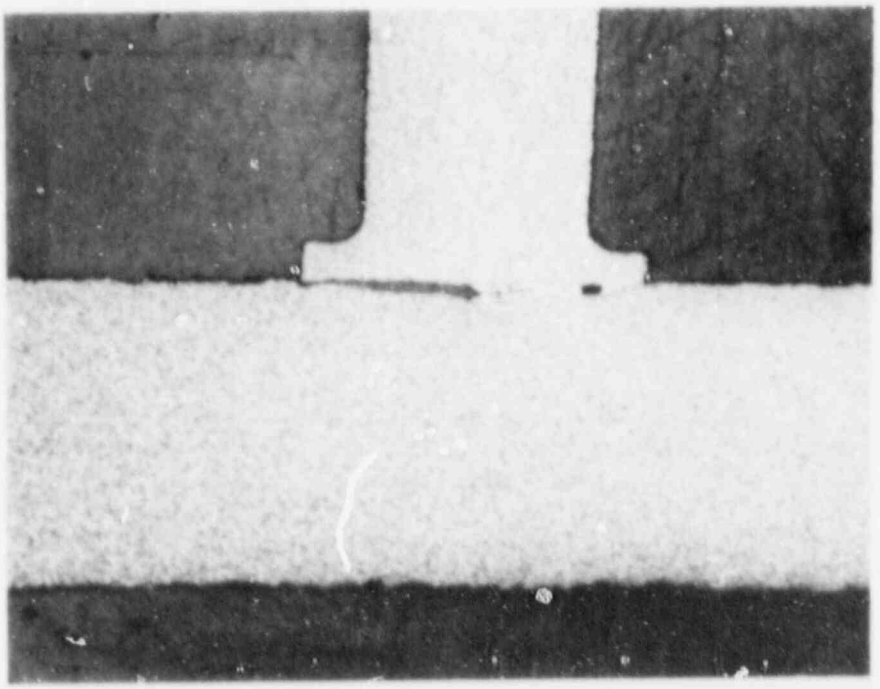

Figure 28 Cross-section of stud weld to insert plate material (8.5x)

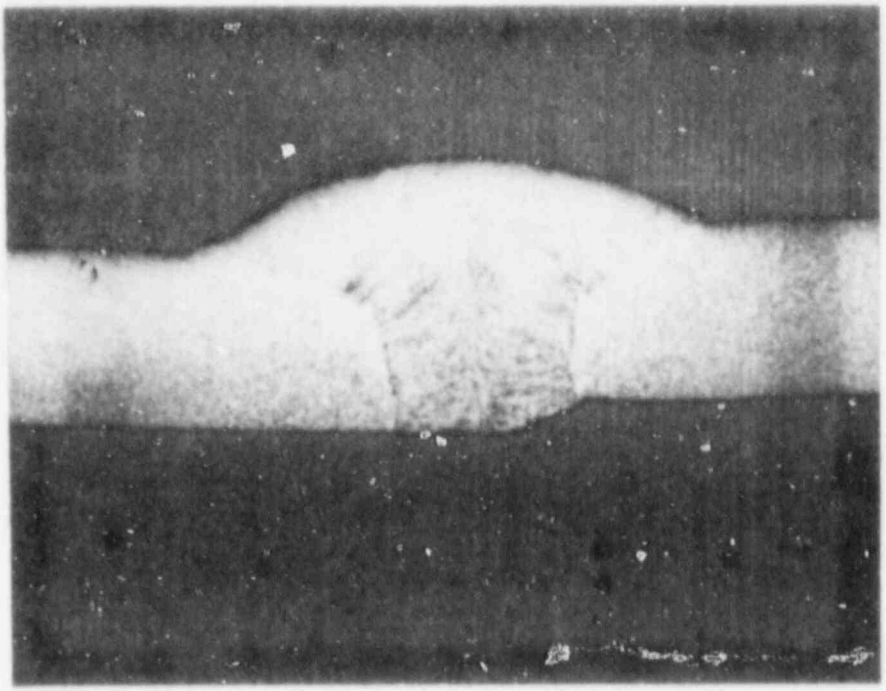

Figure 29 Cross-section of weld between dome sections (flat position 10x)

Figure 30 Cross-section of weld between dome sections (vertical position 12x)

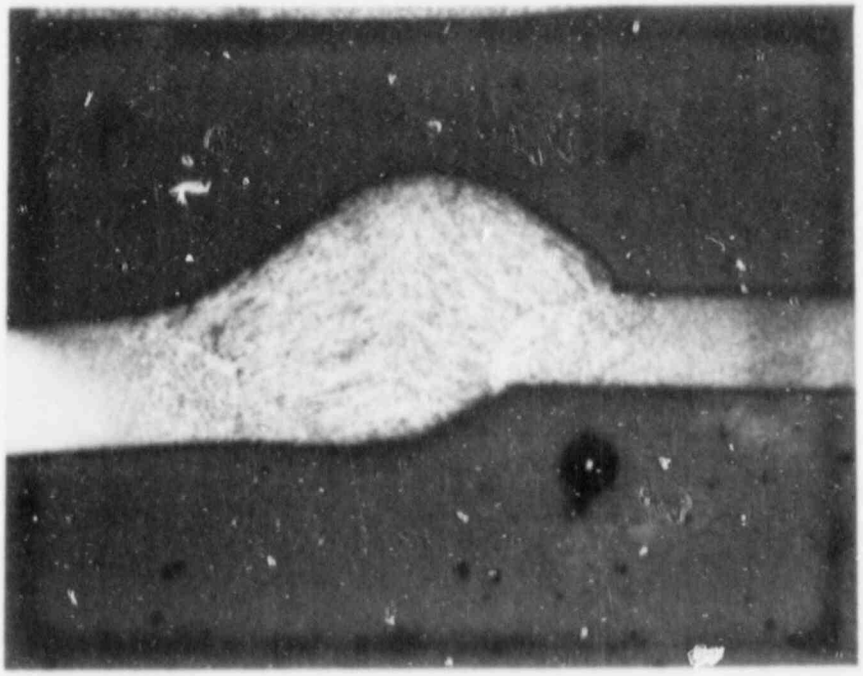

Figure 31 Cross-section of weld between dome and cylinder (horizontal position 8.5x)

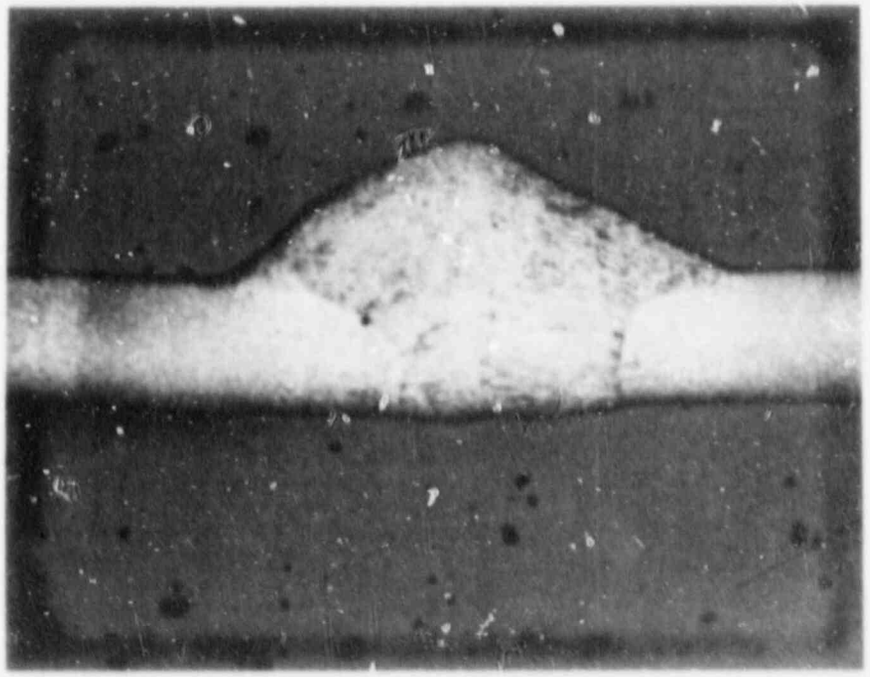

Figure 32 Cross-section of weld between cylinder sections (horizontal position 10x)

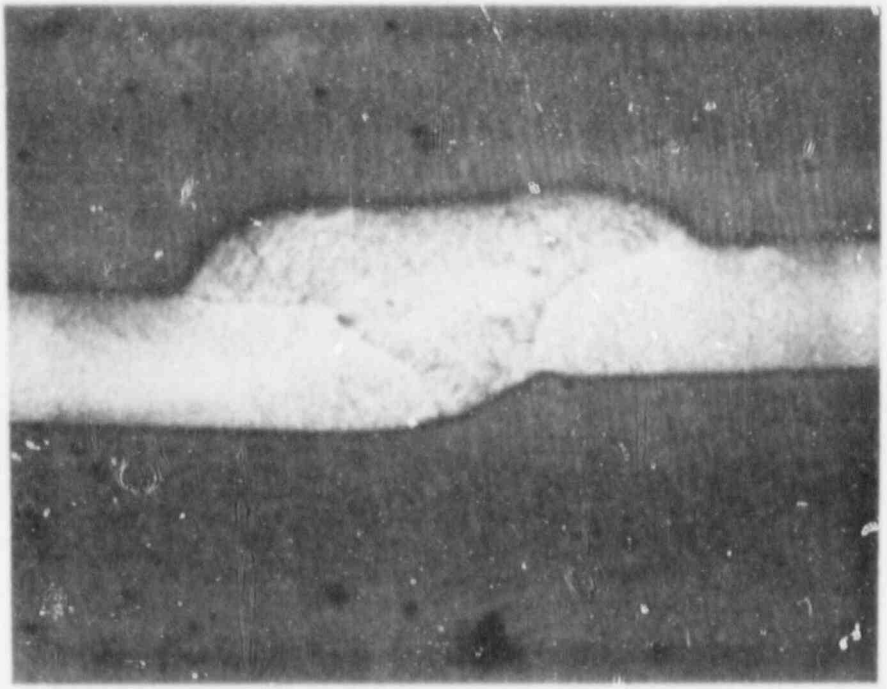

Figure 33 Cross-section of weld between cylinder sections (vertical position 10x)

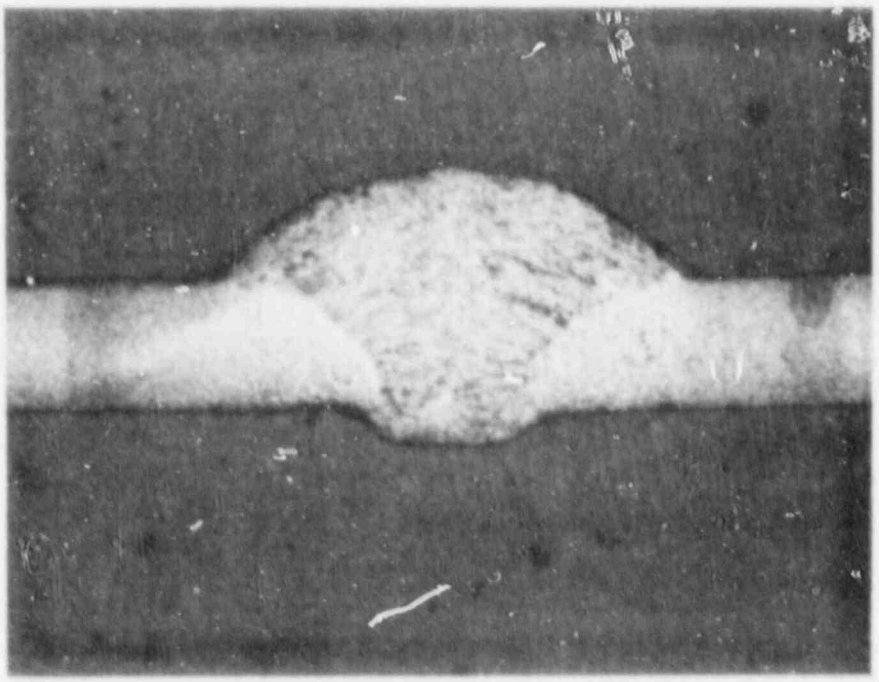

Figure 34 Cross-section of weld between cylinder sections (flat position 10x)

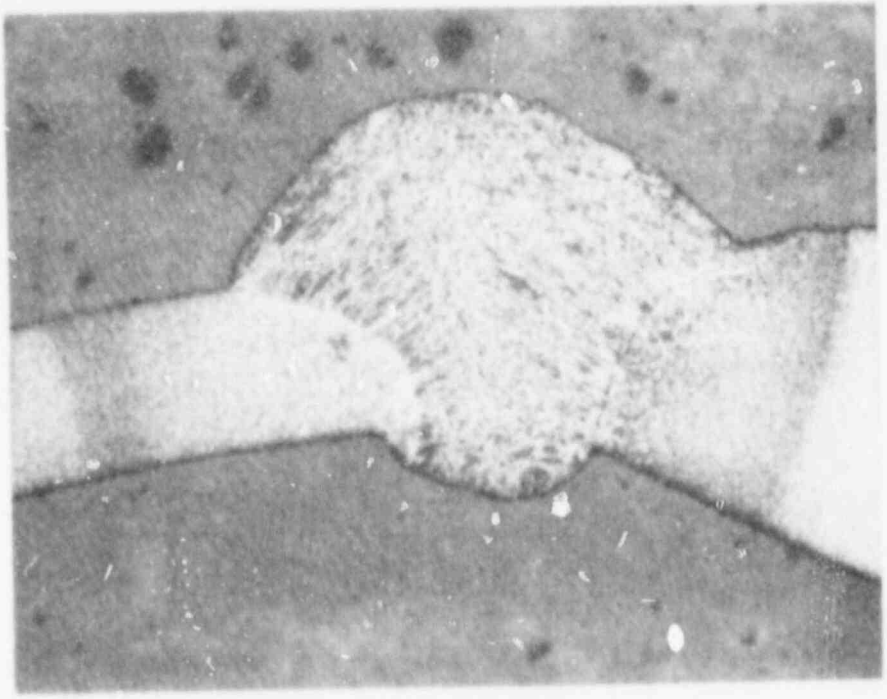

Figure 35 Cross-section of weld between cylinder and insert plate (horizontal position 13x)

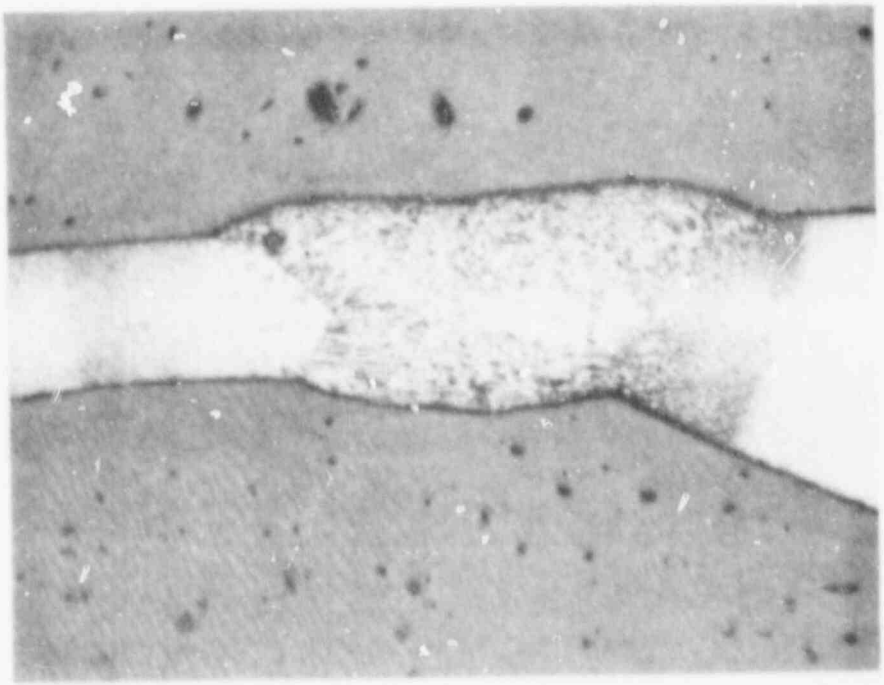

Figure 36 Cross-section of weld between cylinuer and insert plate (vertical position 12x)

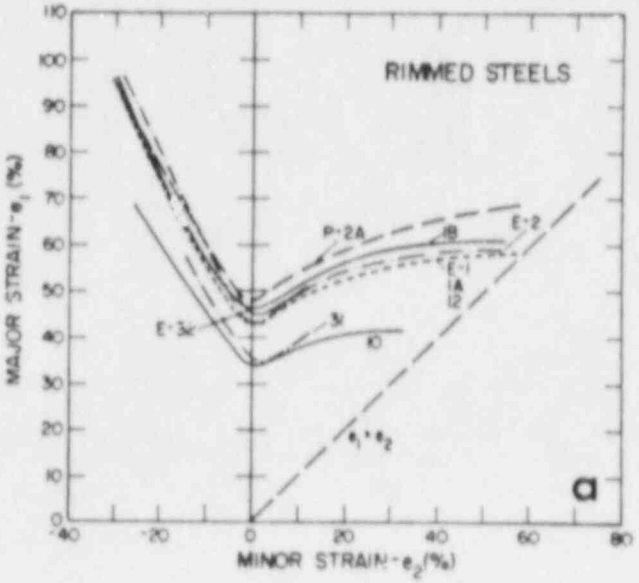

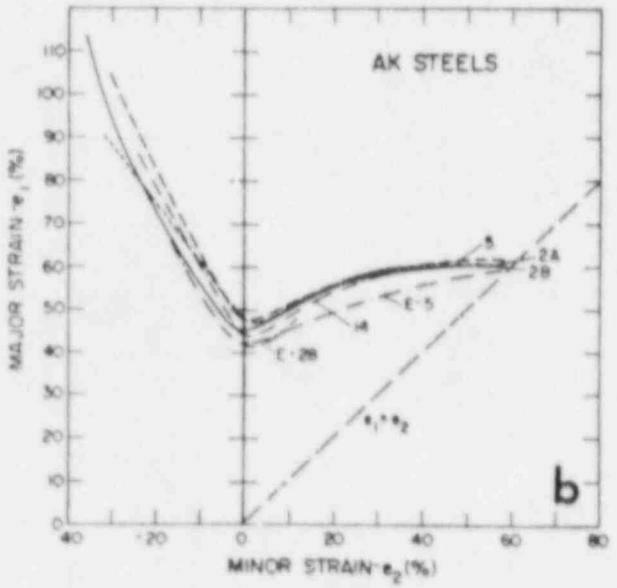

Figure 37 a) Forming limit curves for nine grades and lots of rimmed, low-carbon steels, b) Forming limit curves for six grades and lots of aluminum-killed (AK), low-carbon steels after Hecker (Ref. 3)

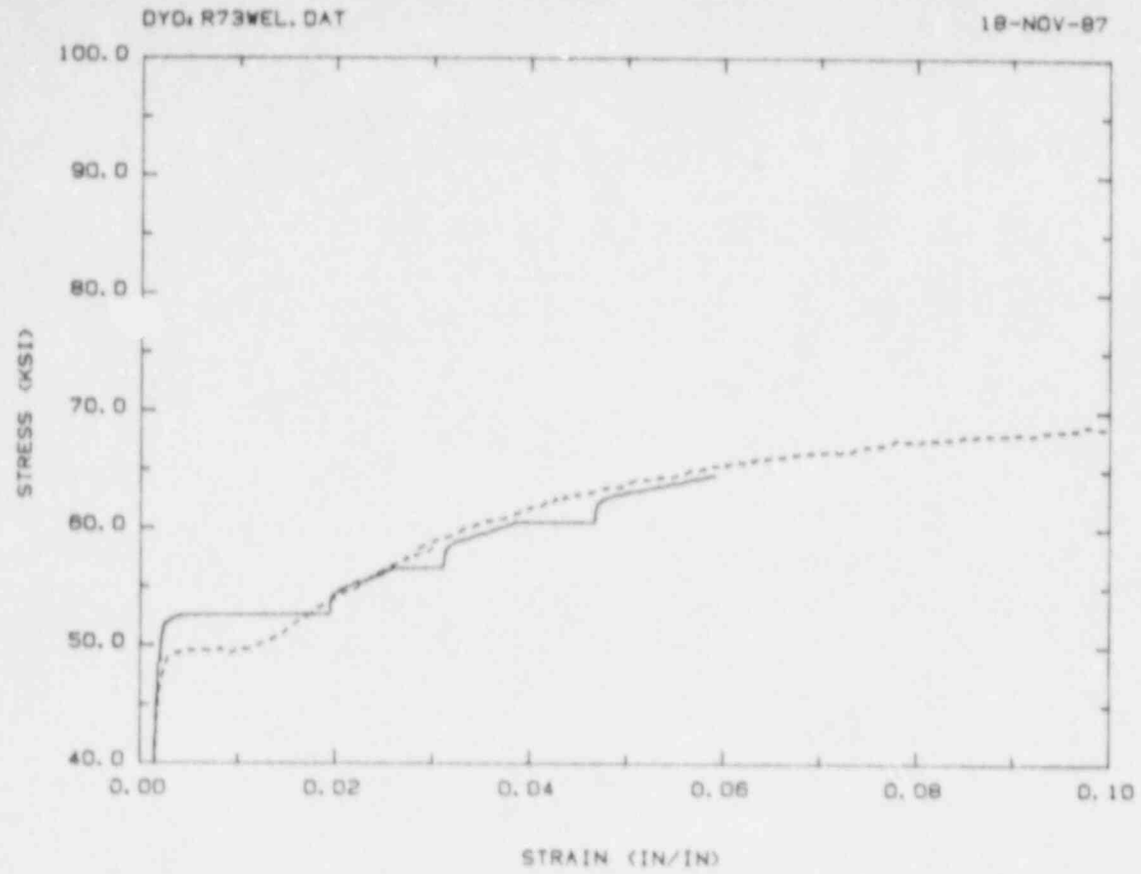

Figure 38 Comparison of monotonic and programmed load tensile behvavior for cylinder material

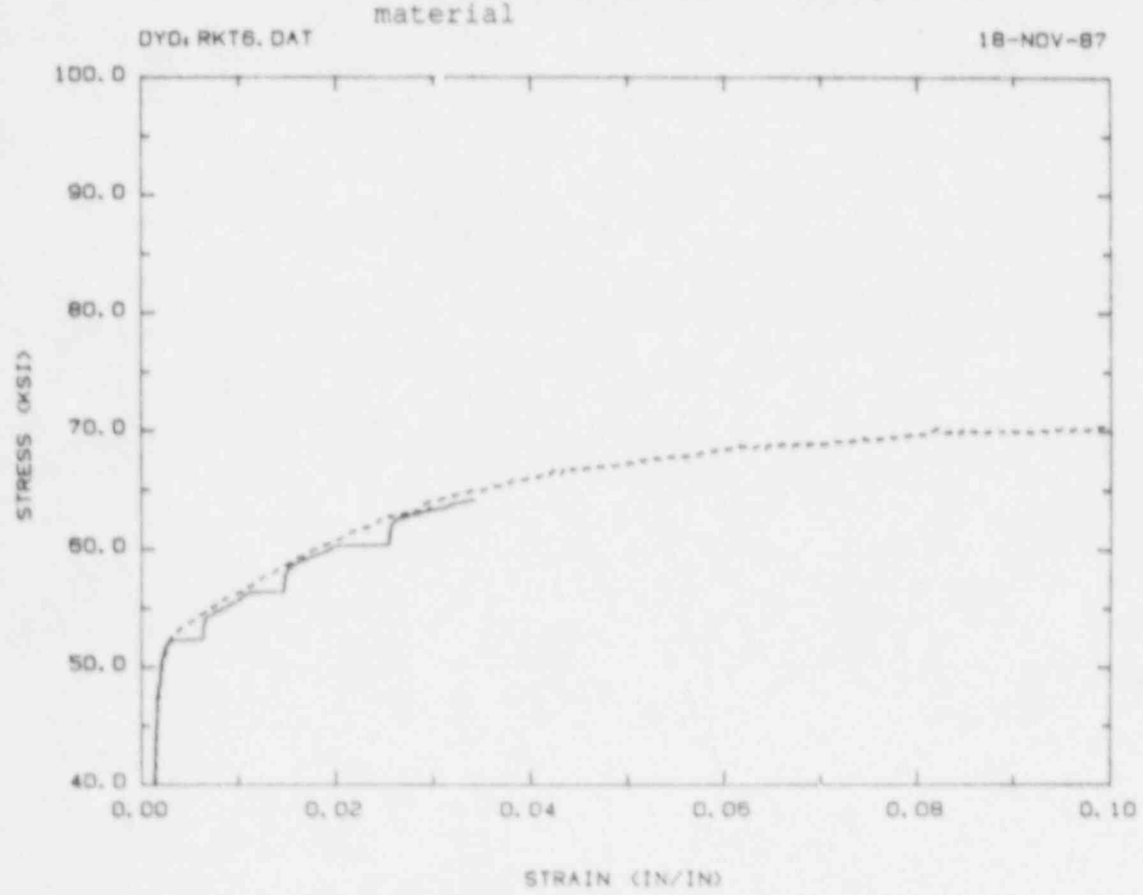

Figure 39 Comparison of monotonic and programmed load tensile behavior for dome material

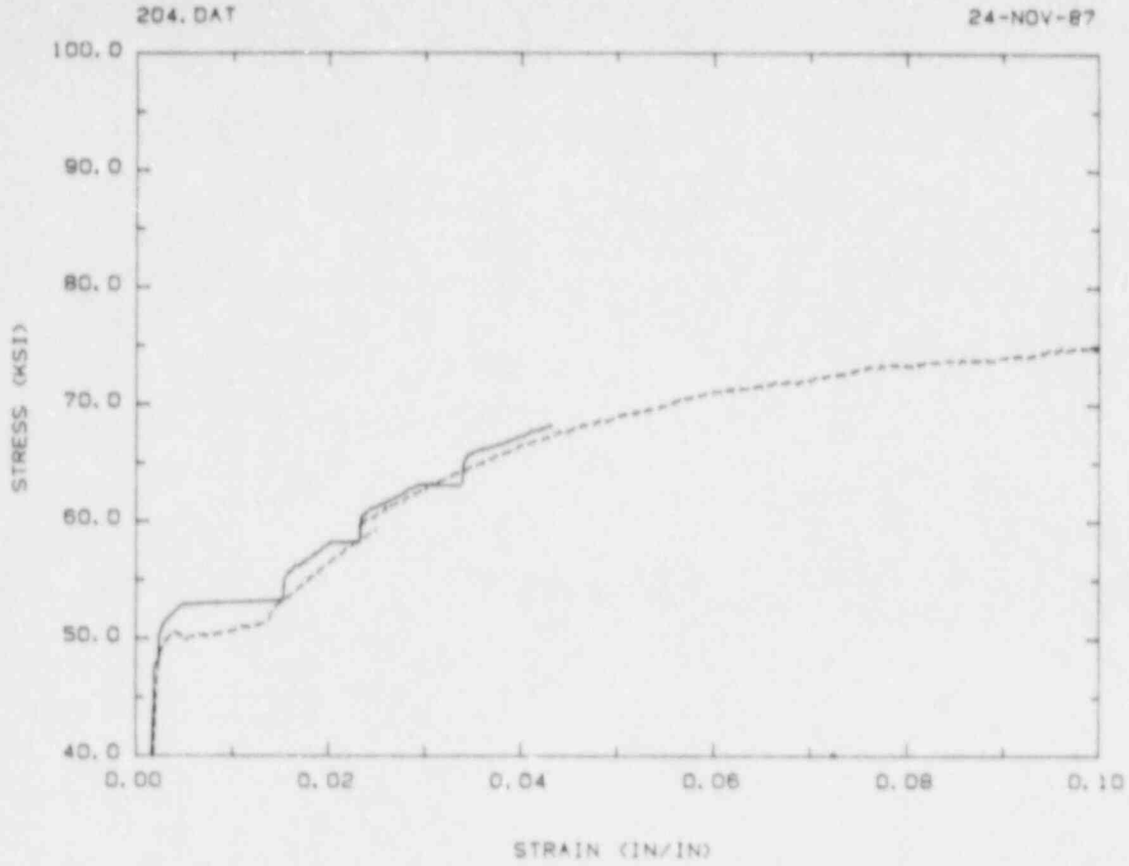

Figure 40 Comparison of monotonic and programmed load tensile behavior for insert plate material

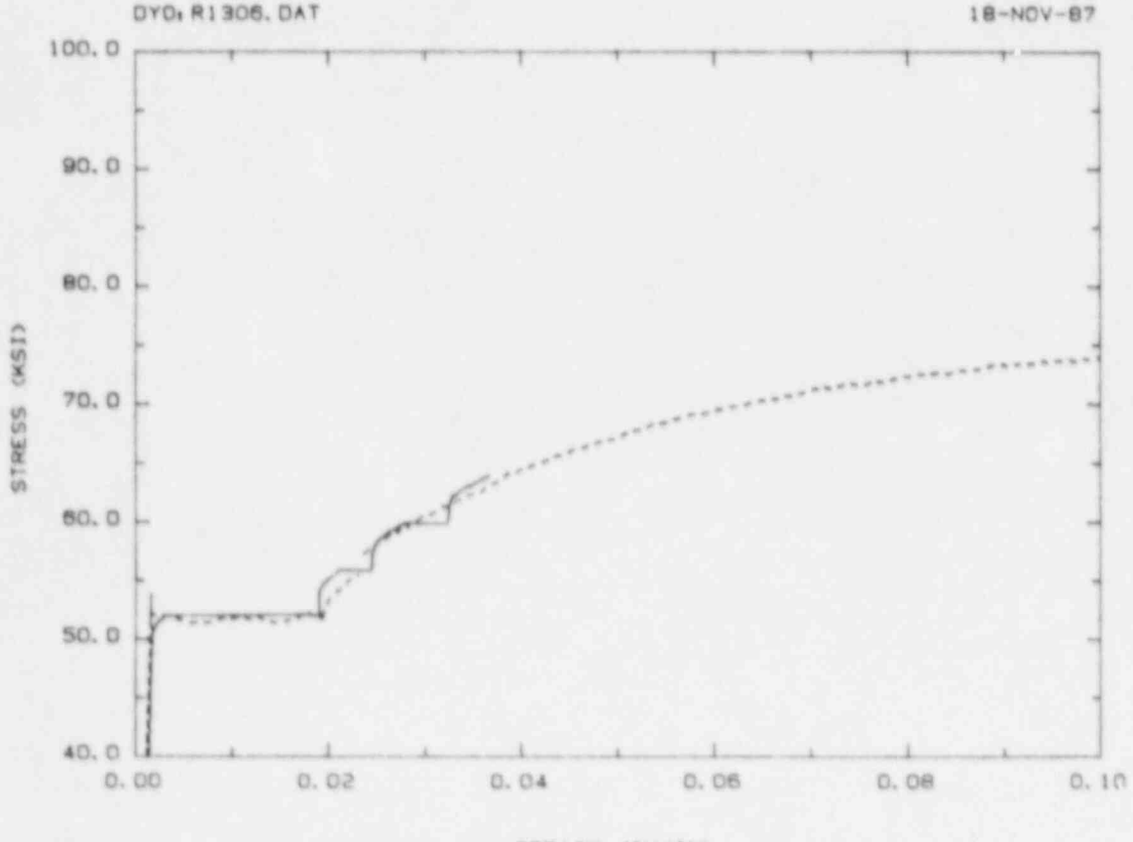

Figure 41 Comparison of monotonic and programmed load tensile behavior for penetration sleeve material

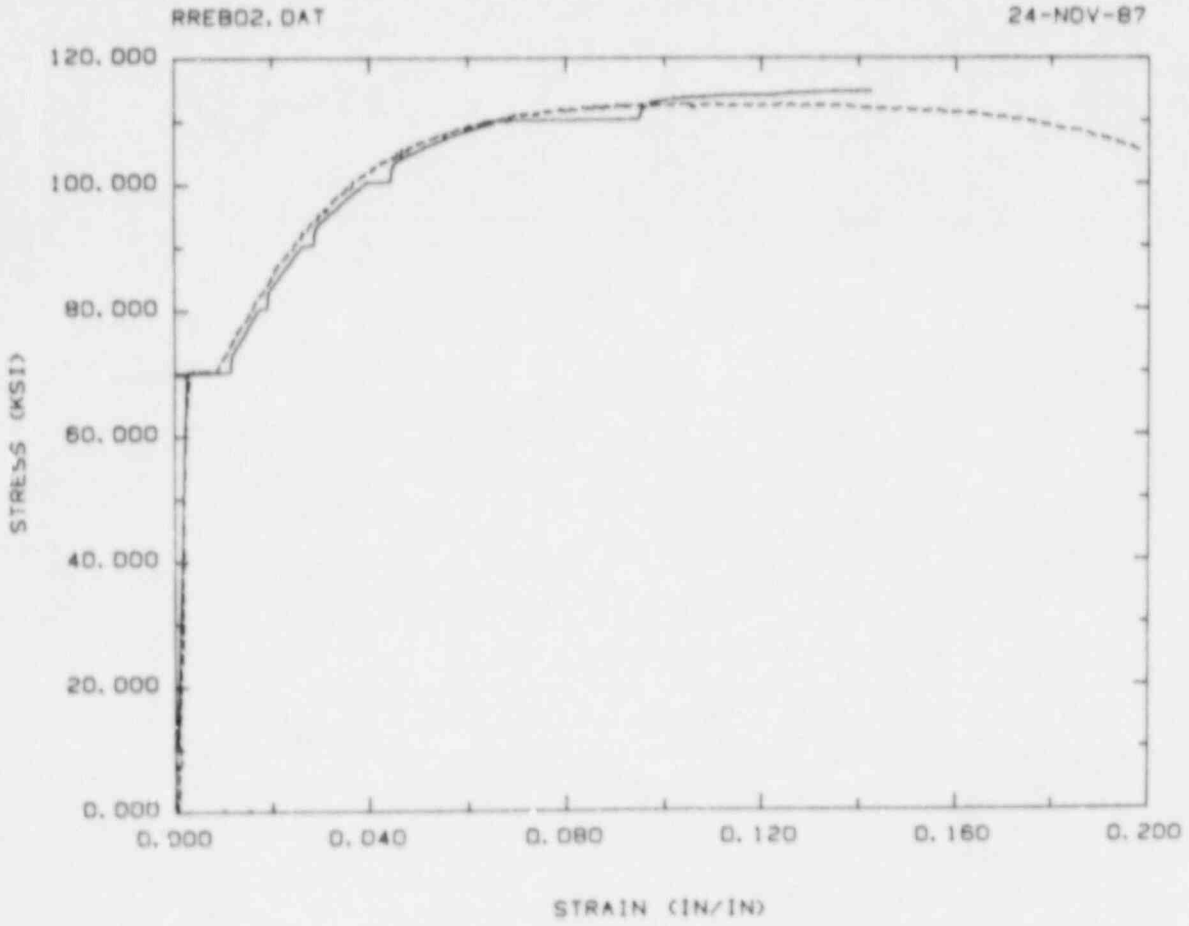

Figure 42 Comparison of monotonic and programmed load tensile behavior for #4 rebar

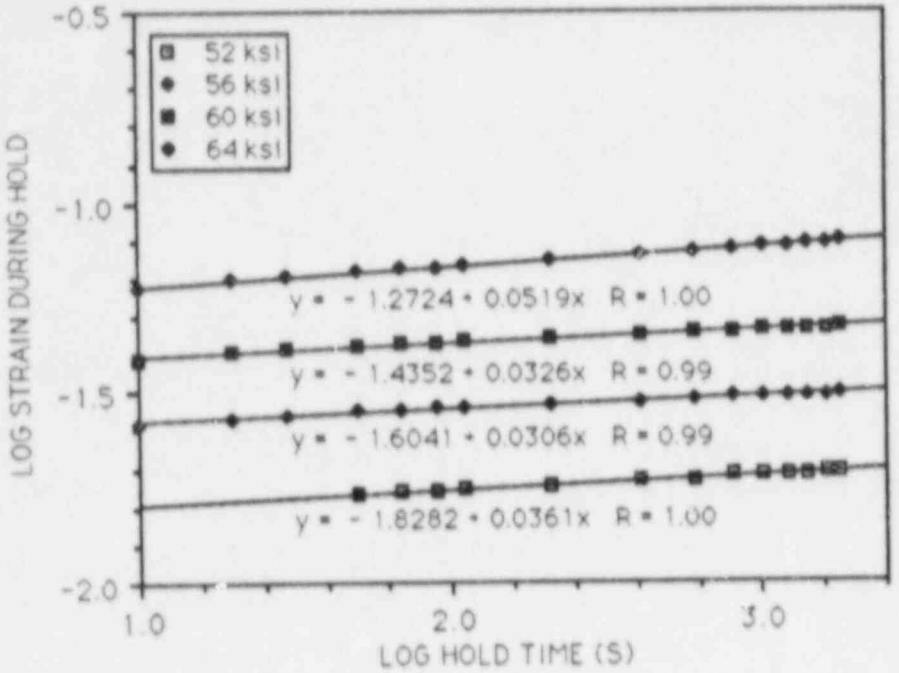

Figure 43 Creep behavior of cylinder material

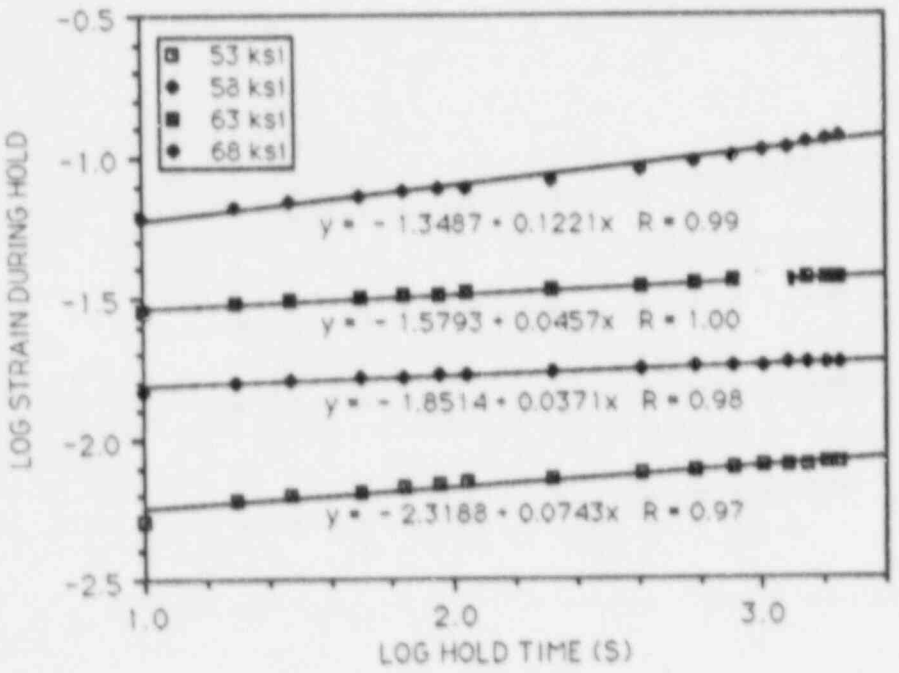

Figure 44 Creep behavior of dome material

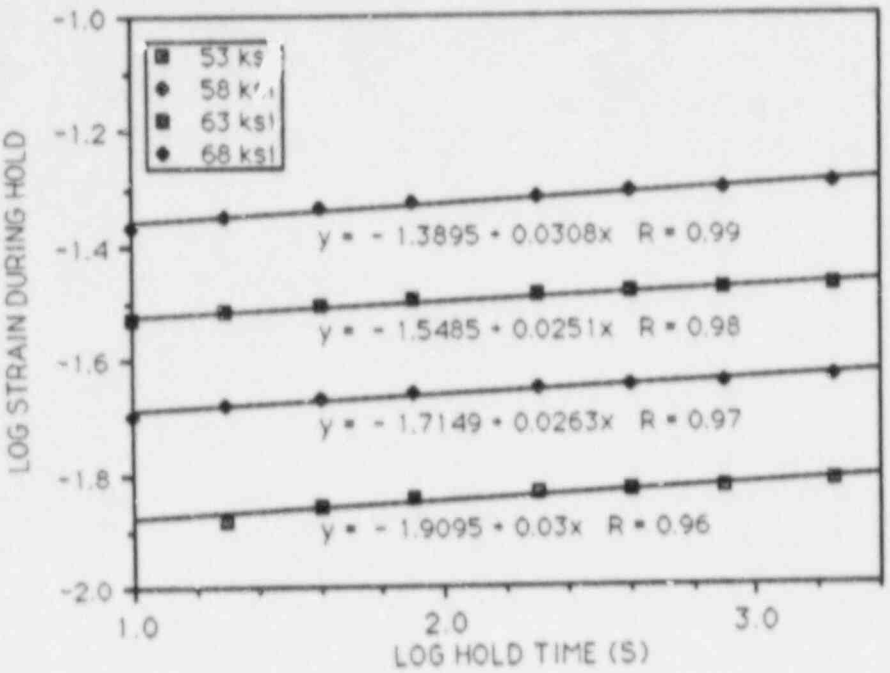

Figure 45 Creep behavior of insert plate material

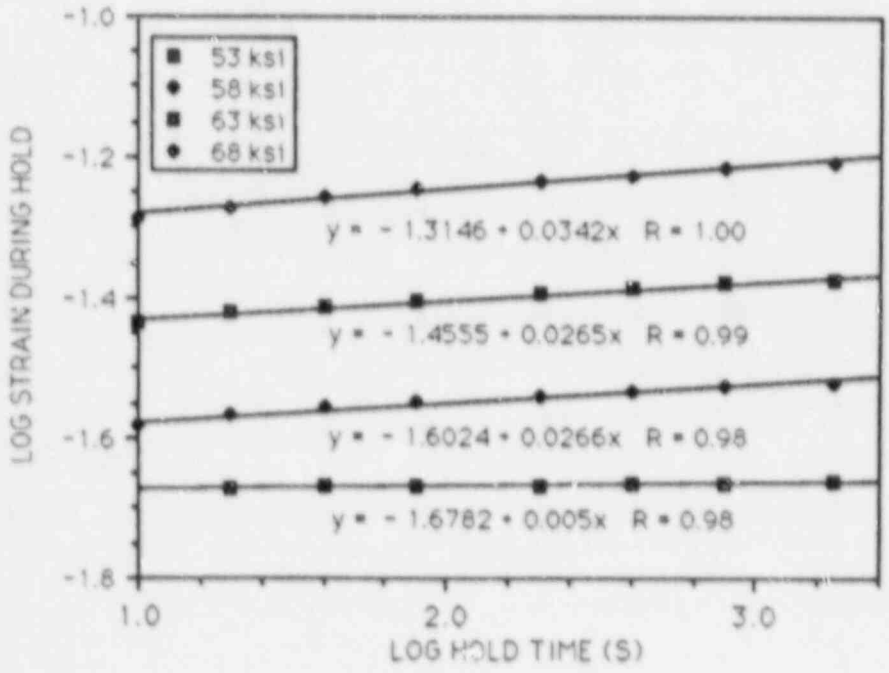

Figure 46 Creep behavior of penetration sleeve material

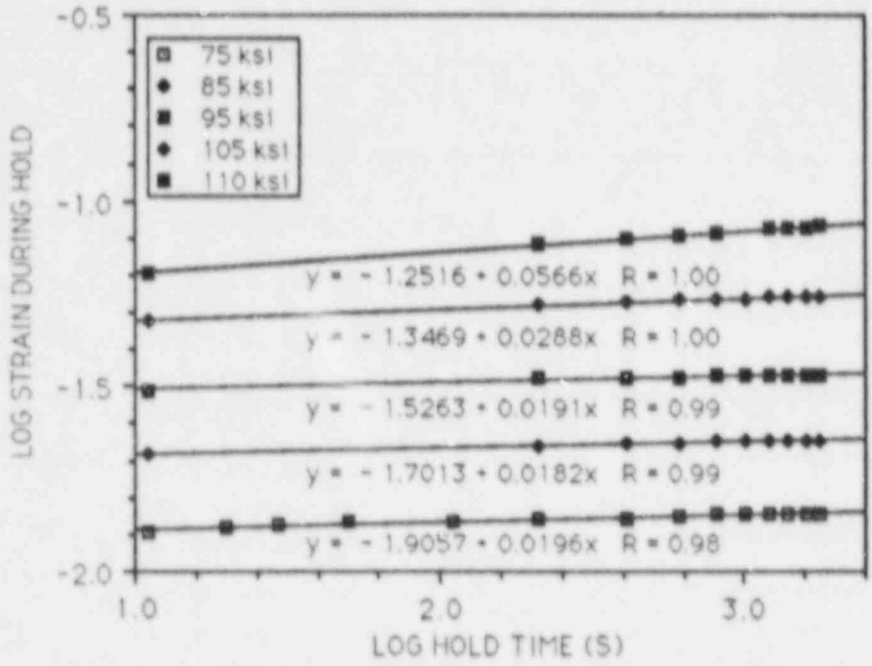

Figure 47 Creep behavior of #4 rebar

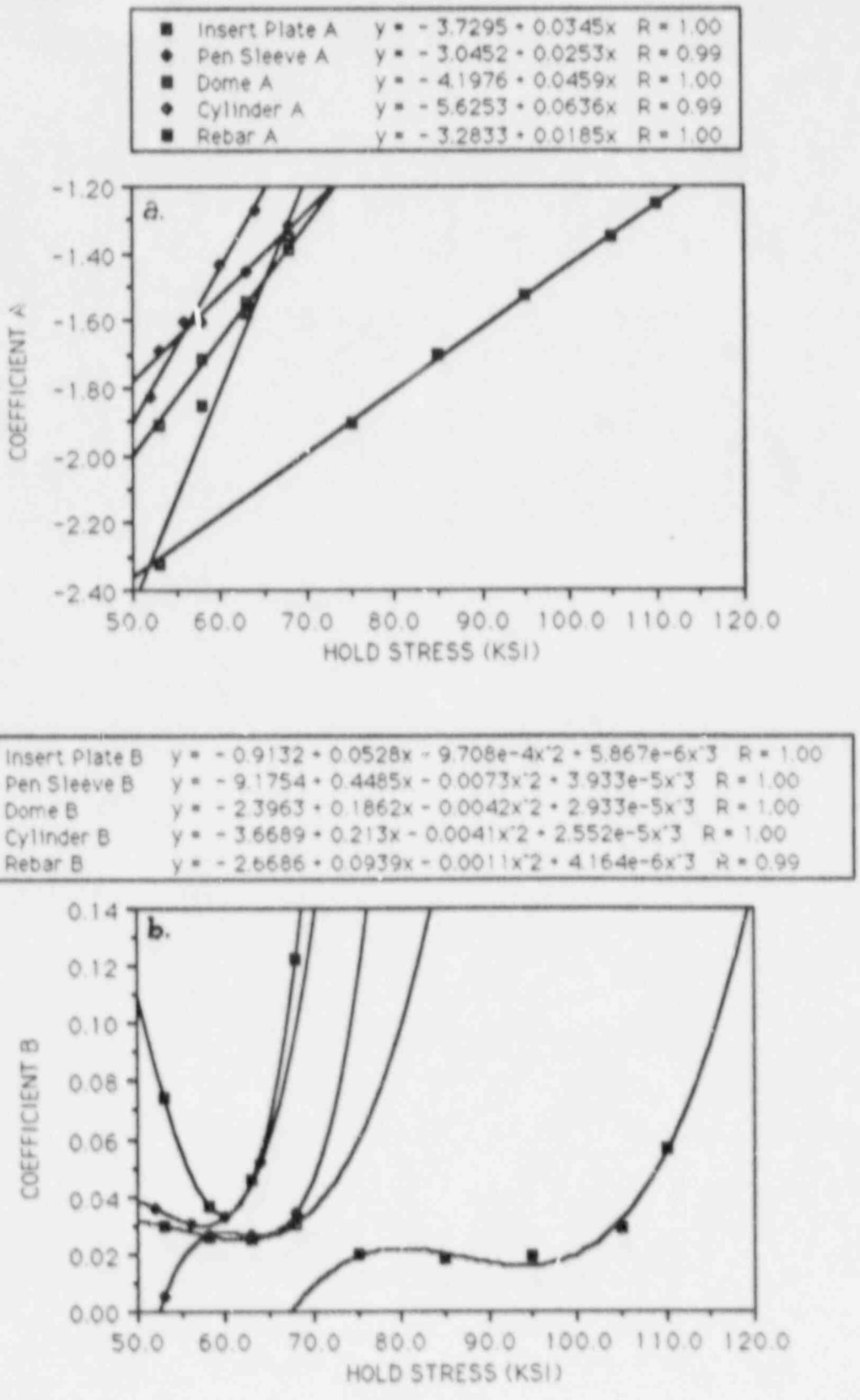

Figure 48 Compilation of creep equation coefficients:
a) Coefficient A,
b) Coefficient B

Distribution:

J. F. Costello (20 Copies)
USNRC/RES
Mail Stop NLS-302
5650 Nicholson Lane
Rockville, MD 20852

H. L. Graves, III
USNRC/RES
Mail Stop NLS-302
5650 Nicholson Lane
Rockville, MD 20852

US Department of Energy
Office of Nuclear Energy
Attn: A. Millunzi
Bernard J. Rock
D. Giessing (3 copies)
Mail Stop B-107
NE-540
Washington, DC 20545

CBI NaCon, Inc.
Attn: Thomas J. Ahl
800 Jorie Boulevard
Oak Brook, IL 60521

Wilfred Baker Engineering
Attn: Wilfred E. Baker
218 E. Edgewood Pl.
P. O. Box 6477
San Antonio, TX 78209

William C. Black
2650 Woodside Road
Bethlehem, PA 18017

Ted M. Brown
701 Stearns Road
Bartlett, Illinois 60103

Battelle Columbus Laboratories
Attn: Richard Denning
505 King Avenue
Columbus, Ohio 43201

Bechtel Power Corporation
Attn: Asadour H. Hadjian
12400 E. Imperial Highway
Norwalk, CA 90650

Bechtel Power Corp.
Attn: T. E. Johnson, Tabir Sen
K. Y. Lee (3 copies)
15740 Shady Grove Rd.
Gaithersburg, MD 20877

City College of New York
Dept. of Civil Engineering
Attn: C. Costantino
140 Street and Convent Ave.
New York, NY 10031

1245 Newmark CE Lab
University of Illinois
Attn: Prof. Mete A. Sozen
208 N. Romine
MC-250
Urbana, IL 61801

Stevenson & Associates
Attn: John D. Stevenson
9217 Midwest Ave.
Cleveland, Ohio 44125

United Engineers & Constructors, Inc.
Attn: Joseph J. Ucciferro
30 S. 17th St.
Philadelphia, PA 19101

Electrical Power Research Institute
Attn: H. T. Tang, Y. K. Tang
Raf Sehgal, J. J. Taylor,
W. Loewenstein (5 copies)
3412 Hillview Avenue
PO Box 10412
Palo Alto, CA 94304

School of Civil & Environ. Engr.
Attn: Professor Richard N. White
Hollister Hall Cornell University
Ithaca, NY 14853

NUTECH
Attn: John Clauss
225 N. Michigan Ave.
16th Floor
Chicago, Illinois 60601

Iowa State University
Department of Civil Engineering
Attn: L. Greimann
420 Town Engineering Bldg.
Ames, IA 50011

TVA
Attn: D. Denton, W9A18
400 Commerce Ave.
Knoxville, TN 37902

Los Alamos National Laboratories
Attn: C. Anderson
PO Box 1663
Mail Stop N576
Los Alamos, NM 87545

EQE Inc.
Attn: M. K. Ravindra
3300 Irvine Aveune
Suite 345
Newport Beach, CA 92660

University of Illinois
Attn: C. Hiess
Dept. of Civil Engineering
Urbana, IL 61801

EBASCO Services, Inc.
Attn: Robert C. Iotti
Two World Trade Center
New York, NY 10048

EG&G Idaho
Attn: N. Barnes, T. L. Bridges
(2 copies)
Willow Creek Bldg. W-3
PO Box 1625
Idaho Falls, ID 83415

Sargent & Lundy Engineers
Attn: A. Walser
P. K. Agrawal (2 copies)
55 E Monroe St.
Chicago, IL 60603

General Electric Company
Attn: E. O. Swain, D. K. Henrie,
B. Gou (3 copies)
175 Curtner Ave.
San Jose, CA 95125

Westinghouse Electric Corp.
Attn: Vijay K. Sazawal
Waltz Mill Site
Box 158
Madison, PA 15663

Quadrex Corporation
Attn: Quazi A. Hossain
1700 Dell Ave.
Campbell, CA 95008

ANATECH International Corp.
Attn: Y. R. Rashid
3344 N. Torrey Pines Court
Suite 320
LaJolla, CA 92037

Oak Ridge National Laboratory
Attn: Steve Hodge
PO Box Y
Oak Ridge, TN 37830

Brookhaven National Laboratory
Attn: C. Hofmayer, T. Pratt
M. Reich (3 copies)
Building 130
Upton, NY 11973

Argonne National Laboratory
Attn: J. M. Kennedy,
R. F. Kulak,
R. W. Seidensticker (3 copies)
9700 South Cass Avenue
Argonne, IL 60439

Tennessee Valley Authority
Attn: Nathaniel Foster
400 Summit Hill Rd.
W9D24C-K
Knoxville, Tennessee 37902

University of Wisconsin
Nuclear Engineering Dept.
Attn: Prof. Michael Corradini
Madison, WI 53706

Brookhaven National Laboratory
Attn: Ted Ginsberg
Building 820M
Upon, NY 11973

Dept. of Chemical & Nuclear Engineering
University of California Santa Barbara
Attn: T. G. Theofanous
Santa Barbara, CA 93106

Northern Illinois University
Mechanical Engineering Dept.
Attn: A. Marchertas
DeKalb, IL 60115

Institut fur Mechanik
Universitaet Innsbruck
Attn: Prof. G. I. Schueller
Technikerstr. 13
A-6020 Innsbruck
AUSTRIA

Nuclear Studies & Safety Dept.
Ontario Hydro
Attn: W. J. Penn
700 University Avenue
Toronto, Ontario
M5G 1X6
CANADA

University of Alberta
Dept. of Civil Engineering
Attn: Prof. D. W. Murray
Edmonton, Alberta
CANADA T6G 2G7

Commissariat a L'Energie Atomique
Centre d'Etudes Nucleaires de Saclay
Attn: M. Livolant, P. Jamet (2 copies)
F-91191 Gif-Sur-Yvette Cedex
FRANCE

Institut de Protection et de
Surete Nucleaire
Commissariat a l'Energie Atomique
Attn: M. Barbe
F-92660 Fontenay-aux-Roses
FRANCE

Kernforschungszentrum Karlsruhe GmbH
Attn: P. Krieg, P. Gast (2 copies)
Postfach 3640
D-7500 Karlsruhe
FEDERAL REPUBLIC OF GERMANY

Lehrstuhl fuer Reaktordynamik
und Reaktorsicherheit
Technische Universitaet Muenchen
Attn: Prof. H. Karwat
D-8046 Garching
FEDERAL REPUBLIC OF GERMANY

Staatliche Materialpruefungsanstalt (MPA)
University of Stuttgart
Attn: Prof. K. F. Kussmaul
Pfaffenwaldring 32
D-7000 Stuttgart 80 (Vaihingen)
FEDERAL REPUBLIC OF GERMANY

Gesellschaft fuer Reaktorsicherheit
Attn: H. Schulz, A. Hoefler,
F. Schleifer (3 copies)
Schwertnergasse 1
D-5000 Koeln 1
FEDERAL REPUBLIC OF GERMANY

Kraftwerk Union AG
Attn: M. Hintergraber
Hammerbacherstr. 12-14
D-8520 Erlangen
FEDERAL REPUBLIC OF GERMANY

Ente Nazionale per l'Energia Elettrica
Attn: Francesco L. Scotto
v. le Regina Margherita, 137
Rome, ITALY

ISMES
Attn: A. Peano
Viale Giulio Cesare 29
I-24100 Bergamo
ITALY

ENEA-DISP
ACO-CIVME
Attn: Giuseppe Pino
Via Vitaliano Brancati, 48
I-00144 Roma
ITALY

Nuclear Equipment Design Dept.
Hitachi Works, Hitachi, Ltd.
Attn: O. Oyamada
3-1-1 Saiwai-Cho
Hitachi-Shi
Ibaraki-ken
JAPAN

Division of Technical Information
Japan Atomic Energy Research Institute
Attn: Jun-ichi Shimobeva
2-2, Uchisaiwai-cho 2-chome
Chiyoda, Tokyo 100
JAPAN

University of Tokyo
Institute of Industrial Science
Attn: Prof. H. Shibata
[illegible] Roppongi 7
[illegible], Tokyo
Japan

Civil [illegible]eering Laboratory
Centr[illegible]search Institute of
Electric Power Industry
Attn: Yukio Aoyagi
1646 Abiko Abiko-Shi Chiba
JAPAN

Kajima Corporation
Attn: K. Umeda
No. 1-1, 2-Chome Nishishinjuku
Shinjuku-ku
Tokyo 160
JAPAN

Muto Institute of Structural Mechanics
Attn: Tadashi Sugano
Room 3005 Shinjuku Mitsui Building
Shinjuku-ku
Tokyo, 163
JAPAN

Nuclear Power Engineering Test Center
Attn: Yoshio Tokumaru
6-2, 3-Chome, Toranomor
Minatoku
Tokyo 105
JAPAN

Japan Atomic Energy Research Inst.
Attn: Kunihisa Soda
Toshikuni Isozaki (2 copies)
Tokai-Mura, Ibaraki-Ken 319-11
JAPAN

Shimizu Construction Co., Ltd.
Attn: Toshihiko Ota
No. 4-17, Etchujima 3-Chome
Koto-Ku
Tokyo 135
JAPAN

Shimizu Construction Co., Ltd.
Attn: Toshiaki Fujimori
No. 18-1, Kyobashi 1-Chome
Chuo-ku
Tokyo 104
JAPAN

Universidad Politecnica
Escuela Tecnica Superior
de Ingenieros Industriales
Attn: Agustin Alonso
Madrid
SPAIN

Principia Espana, SA
Attn: Joaquin Marti
Orense, 36-2
28020 Madrid
SPAIN

Studsvik Energiteknik AB
Attn: Kjell O. Johansson
S-611 82 Nykoping
SWEDEN

Swedish State Power Board
Nuclear Reactor Safety
Attn: Hans Cederberg
Per-Eric Ahlstrom
Ralf Espefaelt (3 copies)
S-162 87 Vallingby
SWEDEN

Swiss Federal Institute of Technology
Institute of Structural Engineering
Attn: W. Ammann
ETH-Hoenggerberg, HIL
CH-8093 Zurich
SWITZERLAND

Motor-Columbus Consulting Engineers, Inc.
Attn: K. Gahler, A. Huber
A. Schopfer (3 copies)
Parkstrasse 27
CH-5401 Baden
SWITZERLAND

EIR (Swiss Federal Institute for
Reactor Research)
Attn: O. Mercier
P. Housemann (2 copies)
CH-5303 Wuerlingen
SWITZERLAND

Swiss Federal Nuclear Safety Inspectorate
Federal Office of Energy
Attn: S. Chakraborty
CH-5303 Wuerenlingen
SWITZERLAND

Swiss Federal Institute of Technology
Attn: Prof. F. H. Wittmann
Chemin de Bellerive 32
CH-1007 Lausanne
SWITZERLAND

Elektrowatt Ingenieurunternehmung AG
Attn: John P. Wolf
Bellerivestr. 36
CH-8022 Zurich
SWITZERLAND

Atomic Energy Establishment
Attn: Peter Barr
Winfrith
Dorchester Dorset
DT2 8DH
UNITED KINGDOM

Atomic Energy Authority
Safety and Reliability Directorate
Attn: D. W. Phillips
Wigshaw Lane
Culcheth
Warrington WA3 4NE
UNITED KINGDOM

HM Nuclear Installation Inspectorate
Attn: R. J. Stubbs
St. Peter's House
Stanley Precinct
Bootle L20 3LZ
UNITED KINGDOM

Taylor Woodrow Construction Limited
Attn: Carl C. Fleischer
Richard Crowder (2 copies)
345 Ruislip Road
Southall, Middlesex
UB1 2QX
UNITED KINGDOM

Central Electricity Generating Board
Attn: J. Irving
Barnett Way
Barnwood, Gloucester
GL4 7RS
UNITED KINGDOM

Central Electricity Generating Board
Attn: Carl Lomas
Booths Hall
Chelford Road
Knutsford, Cheshire
WA16 8QG
UNITED KINGDOM

1520 C. W. Peterson
1521 R. D. Krieg
1521 J. R. Weatherby
1832 P. W. Hatch
1833 G. A. Knorovsky (5)
3141 S. A. Landenberger (5)
3151 W. I. Klein
6400 D. J. McCloskey
6410 N. R. Ortiz
6420 J. V. Walker
6440 D. A. Dahlgren
6442 W. A. von Riesemann (21)
6442 D. S. Horschel (5)
6447 M. P. Bohn
6448 D. L. Berry
7540 T. S. Church
7542 T. G. Priddy
8524 P. W. Dean

NRC FORM 335 (2-84) NRCM 1102, 3201, 3202

U.S. NUCLEAR REGULATORY COMMISSION

BIBLIOGRAPHIC DATA SHEET

SEE INSTRUCTIONS ON THE REVERSE

1 REPORT NUMBER (Assigned by TIDC, add Vol. No., if any)

NUREG/CR-5099
SAND88-0052

2 TITLE AND SUBTITLE

Evaluation of Materials of Construction for the Reinforced Concrete Reactor Containment Model

3 LEAVE BLANK

4 DATE REPORT COMPLETED

MONTH	YEAR
August	1988

5 AUTHOR(S)

G. A. Knorovsky
P. W. Hatch
M. R. Gutierrez

6 DATE REPORT ISSUED

MONTH	YEAR
September	1988

7 PERFORMING ORGANIZATION NAME AND MAILING ADDRESS (Include Zip Code)

Sandia National Laboratories
Albuquerque, NM 87185

8 PROJECT/TASK/WORK UNIT NUMBER

9 FIN OR GRANT NUMBER

FIN No. A1249

10 SPONSORING ORGANIZATION NAME AND MAILING ADDRESS (Include Zip Code)

Division of Engineering
Office of Nuclear Regulatory Research
U.S. Nuclear Regulatory Commission
Washington, DC 20555

11a TYPE OF REPORT

Technical

b PERIOD COVERED (Inclusive dates)

12 SUPPLEMENTARY NOTES

13 ABSTRACT (200 words or less)

This report summarizes the chemical analysis, metallography, and tensile test results obtained from steel materials and welds used in the construction of a 1/6-scale model reinforced concrete nuclear reactor containment. The purpose of building such a model is to experimentally verify the ability of numerical models to predict deformation and failure in full-size containments. Naturally, the predictions of such models are strongly influenced by the constitutive models used for the containment materials. The program reported on here was intended to provide such data. Besides providing tensile test data on the sheet, plate, and rebar materials used for dome, cylinder, cylinder inserts, reinforcements, & penetrations, pull tests on several weld geometries have been obtained. Standard tensile test data derived from load vs. extensometer output records (i.e. engineering stress vs. engineering strain) are supplemented with true stress vs. true strain data collected by measuring actual cross sectional areas during interrupted tensile tests. Additionally, "r" value measurements (ratio of width to thickness strain) which can be used to provide information about anisotropic multiaxial flow conditions are derived from the true strain data and reported. A small number of tests which included holds at constant load levels were also performed and analyzed to yield ambient temperature creep equations. Finally, conditions resulting from construction practices (such as residual stresses and the Bauschinger effect) which may affect the prediction of yield and fracture stresses from this data are briefly discussed.

14 DOCUMENT ANALYSIS - a KEYWORDS/DESCRIPTORS

reinforced concrete
chemical analysis
numerical model

b IDENTIFIERS/OPEN ENDED TERMS

15 AVAILABILITY STATEMENT

Unlimited

16 SECURITY CLASSIFICATION

(This page)
Unclassified
(This report)
Unclassified

17 NUMBER OF PAGES

18 PRICE

NUREG/CR-5099

EVALUATION OF MATERIALS OF CONSTRUCTION FOR THE REINFORCED CONCRETE REACTOR CONTAINMENT MODEL

SEPTEMBER 1988